Review

Imaging single cells in the living retina

David R. Williams *

Center for Visual Science, William G. Allyn Professor of Medical Optics, University of Rochester, Box 270270, Rochester, NY 14627-0270, United States

ARTICLE INFO

ABSTRACT

A quarter century ago, we were limited to a macroscopic view of the retina inside the living eye. Since then, new imaging technologies, including confocal scanning laser ophthalmoscopy, optical coherence tomography, and adaptive optics fundus imaging, transformed the eye into a microscope in which individual cells can now be resolved noninvasively. These technologies have enabled a wide range of studies of the retina that were previously impossible.

1. Introduction

The ability to look inside the living human eye is central to our understanding of how the normal eye works and the diseased eye fails. This article focuses on technological advances in the spatial resolution of retinal imaging during the last quarter century and some of the scientific discoveries they have made possible. These advances have transformed retinal imaging from a macroscopic to a microscopic modality in which individual cells can now be resolved. There are many books and review articles that address these advances. Relevant books include (Huang, Kaiser, Lowder, & Traboulsi, 2006; Masters & Thompson, 2001; Porter, Queener, Lin, Thorn, & Awwal, 2006; Schuman, Puliafito, & Fujimoto, 2004) and review articles include Costa et al. (2006), Drexler and Fujimoto (2008), Fujimoto (2003), Godara, Dubis, Roorda, Duncan, and Carroll (2010), Hampson (2008), Miller, Kocaoglu, Wang, and Lee (2011), Miller and Roorda (2009), chap. 17, Podoleanu (2005), Podoleanu and Rosen (2008), Roorda (2010), Rossi et al. (2011), Wilt et al. (2009), Wojtkowski (2010).

It has never been easy to peer inside the living eye. Though several investigators in the 19th century were aware of the illumination conditions necessary to cause the otherwise impenetrable pupil to glow red, they failed to obtain a clear view of the living retina until Helmholtz invented the ophthalmoscope (Helmholtz, 1851). Since then, the evolution of this instrument has been punctuated by important, if occasional, technical advances such as adding a camera that could record retinal images on film (Jackman &

Webster, 1886). Surprisingly, before the late 1980s there were few improvements in optical resolution since Helmholtz's landmark invention. A rare example is the incorporation of the electronic flash, invented ∼30 years earlier by Edgerton, that allowed exposures brief enough to avoid eye motion blur (Ogle & Rucker, 1953). In contrast, the last quarter century has witnessed gains in spatial resolution that have completely transformed our capacity to recover information from the retinal image.

2. The first glimpses of retinal cells in the living eye

The fact that ophthalmoscopy lacked the resolution to see single cells a quarter of a century ago did not preclude drawing inferences about the effects of single cells on vision well before then. Perhaps the best example is the brilliant paper of Hecht, Schlaer, and Pirenne (1942) in which they concluded that ∼10 photons are required to detect a flash at absolute threshold. Because these 10 quantal absorptions almost certainly occurred in 10 different receptors, they could conclude that absorption of one photon of light was sufficient to excite a single rod. Their argument was necessarily a statistical one because the poor optical quality of the eye precludes stimulating one and only one rod in the human eye. However, there is another class of photoreceptor, the short wavelength sensitive cones, that are rare enough in the retina that a focused point source, suitably arranged to stimulate only that class of cell, can stimulate only one cell at a time. Capitalizing on this unique aspect of this cone submosaic, MacLeod, Hayhoe and I (Williams, MacLeod, & Hayhoe, 1981) showed that subjects could reliably detect a flash of light that stimulated a single cone photoreceptor.

These experiments lead to psychophysical methods to characterize the arrangement and spacing of cones that relied on aliasing effects caused by imaging interference fringes on the retina (Williams, 1985, 1988). Artal and Navarro (1989) wondered whether another variant of interferometry, based on the interference of light returning from the retina rather than light entering the eye, could be used to estimate the spacing of cones in the living eye. Their approach was derived from a technique used in astronomy, stellar speckle interferometry, that had been developed to recover high spatial frequency information from speckled images, such as whether an object in the sky was a single or a binary star (Labeyrie, 1970). They collected images of the speckle patterns generated by illuminating small patches of living human retina with coherent light. The average power spectrum of multiple images revealed a ring corresponding to spatial frequency components of the cone mosaic, providing the first evidence about the granularity of the cone mosaic obtained from images of the living human eye.

Unfortunately, Artal and Navarro's method did not allow for the direct observation of the cone mosaic because the cones are obscured by the interference of the coherent light reflected from multiple layers of the retina. Experiments in animals had previously demonstrated direct imaging of receptors. In 1985, Land and Snyder (1985) showed in the snake and Jagger (1985) showed in the cane toad that it is possible to image photoreceptor cells through the natural optics of the intact eye. While these observations were made on animal eyes with good optics and unusually large receptors, they encouraged the possibility that this could also be achieved in the human eye. Cideciyan and Jacob (1994) noticed small bright spots in fundus images from patients who were carriers of x-linked retinitis pigmentosa. They speculated that these spots were cones back-illuminated by the highly-reflective tapetum-like fundus in these patients.

Miller, Williams, Morris, and Liang (1996) constructed a custom fundus camera specifically designed to search for single cones in the normal human eye. This camera illuminated the retina with a small, ~7 min of arc, field of monochromatic light. To avoid speckle, the laser source used was deliberately rendered incoherent with a spinning diffuser. Careful attention was paid to the correction of defocus and astigmatism. With this instrument they obtained the first direct images of the cone mosaic in the normal living human eye, examples of which are shown in Fig. 1. Cones continue to be a favorite target for retinal microscopy because they act like tiny waveguides, and the light that enters them is preferentially redirected back through the pupil, producing a high contrast mosaic of bright spots in the retinal image. There is a common misconception that additional optical techniques such as adaptive optics are required to image the cone mosaic in the living eye, but Miller et al. showed, and many others have since confirmed (e.g. Pircher, Baumann, Göttzinger, & Hitzenberger, 2006; Vohnsen, Iglesias, & Artal, 2004; Wade & Fitzke, 1998), that cellular imaging is possible outside the foveal center in young eyes with good optical quality and careful correction of defocus and astigmatism alone. These early glimpses of structures as small as single cones in the living human eye encouraged the development of new technologies, especially adaptive optics, to improve the resolution of retinal imaging.

3. The scanning laser ophthalmoscope

The invention of the scanning laser ophthalmoscope (SLO) by Webb, Hughes, and Pomerantzeff (1980) represented a radical departure from the design of conventional fundus cameras of the time and laid the groundwork for modern retinal microscopy. They developed what they called initially a "flying spot TV ophthalmo-

Fig. 1. The first images taken of the human photoreceptor mosaic in the human eye with a high magnification fundus camera and the method developed by Miller et al. (1996). (A) Image obtained at 0.5° from the foveal center. (B) Image obtained at 2.5° from the foveal center.

scope" that raster-scanned a single laser spot onto the retina, collecting the returning light onto a detector with much greater sensitivity than film. The use of a dilated pupil to collect the light and a photomultiplier tube for light detection made it possible to collect video images of the retina with significantly less light exposure than the conventional film-based fundus cameras of the time. In 1987, Webb, Hughes, and Delori introduced the principle of confocal detection into an improved SLO. Minsky (1957), better known for his contributions to artificial intelligence, first proposed the idea of confocal imaging in a patent for a scanning microscope. Surprisingly, it took 30 years for this simple and effective principle to find its way from microscopy into ophthalmoscopy. The confocal SLO used the same optical path for scanning the laser spot on the retina and for delivering the returning light to the detector, as shown in Fig. 2. This double passage of light through the scanning mirrors produced a stable image at the detector of the scanned spot on the retina. A confocal pinhole just in front of the light detector collected most of the light from the retina while rejecting light originating from planes other than the retina. Though the instrument did not improve lateral resolution over that which could be achieved with conventional fundus cameras of the day, it did improve axial resolution, significantly increasing image contrast. As shown in Fig. 3, the axial resolution of the confocal SLO was about 300 μm, modest by today's standards, but it represented
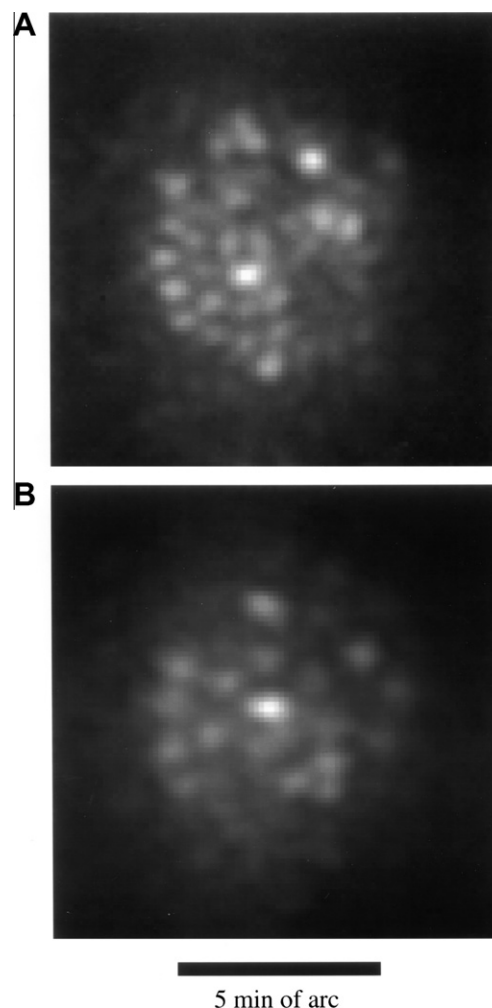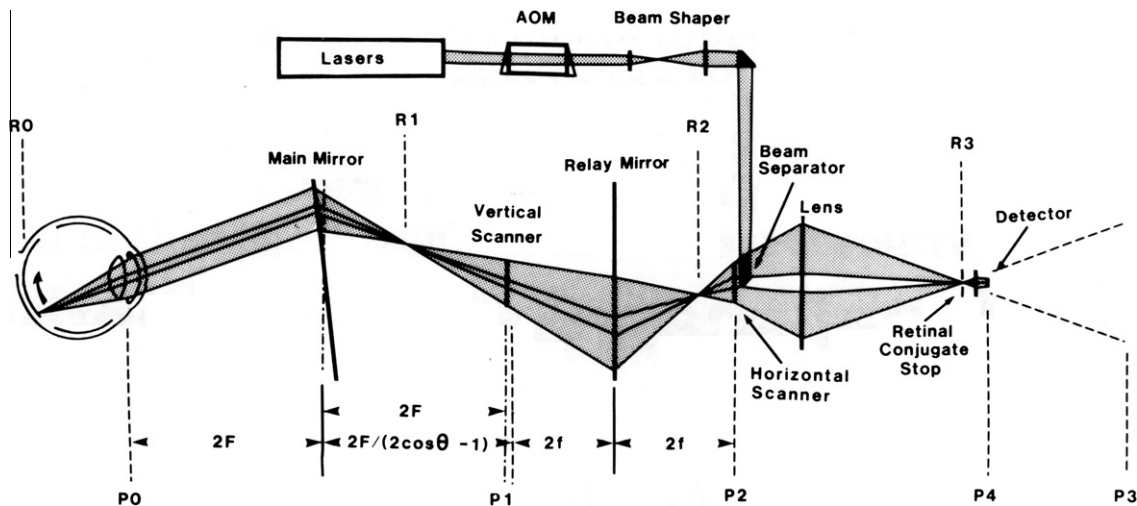
Fig. 2. Optical layout of the first confocal SLO. The light path is shown at one instant in time. Mirrors are shown as transmissive for simplicity. Pupil conjugate planes are labeled with P_n. P_3 is a virtual image of the pupil, converted to a real image at P_4 by a microscope objective. Retinal conjugate planes are labeled with R_n. R_3 corresponds to the confocal pinhole just in front of the light detector. From Webb, Hughes, and Delori (1987).
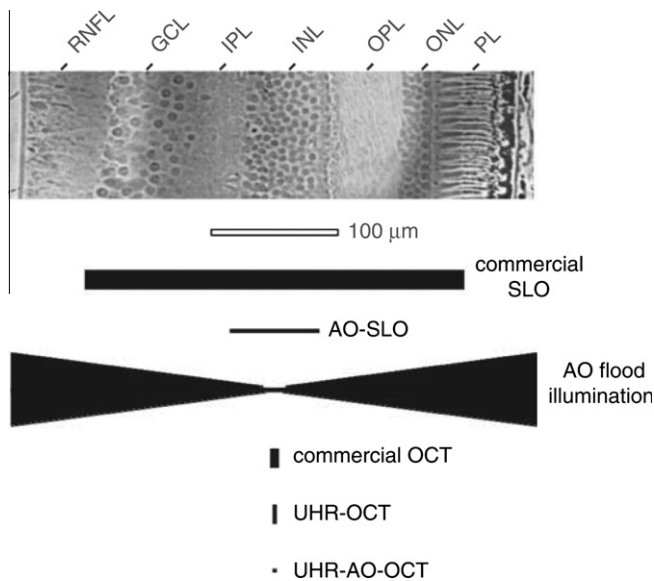

Fig. 3. Comparison of (top) cell size in a histological cross section of the human retina with (bottom) the resolving capability of the major types of retinal imaging modalities with and without AO. The vertical and horizontal dimensions of the solid black symbols denote, respectively, the lateral and axial resolution of the instruments. Examples shown include the commercial confocal scanning laser ophthalmoscope (SLO), adaptive optics confocal scanning laser ophthalmoscope (AOSLO), adaptive optics flood illumination, commercial OCT, ultrahigh-resolution OCT (UHR-OCT), and ultrahigh-resolution OCT with adaptive optics (UHR–AO-OCT). GCL, ganglion cell layer; IPL, inner plexiform layer; INL, inner nuclear layer; OPL, outer plexiform layer; ONL, outer nuclear layer; PL, photoreceptor layer; RNFL, retinal nerve fiber layer. From Miller (2011).

the first improvement in resolution since the flash tube prevented eye motion blur. Moreover, the scanning technology and confocal detection method introduced by Webb and his colleagues were key elements of many of the high resolution, microscopic retinal imaging technologies that were soon to follow.

4. Improvements in axial resolution through OCT

The fundus cameras and confocal SLOs ca. 1990 were designed on the premise that light is made of particles that travel in straight lines. Though the wave nature of light had been proposed by Huygens (1678) and confirmed by Young's famous double slit interference experiment (1804), it had yet to impact methods to image the retina. But in the 1990s, optical coherence tomography harnessed the wave nature of light, thereby achieving an unprecedented axial resolution in retinal images. The retina is a three-dimensional structure from 100 to 400 μm thick that is organized into distinct layers of cells and the synaptic connections between them. Each layer has a specific role in the circuitry that transforms the retinal image into signals the brain can interpret, and each can be affected differently in retinal disease. OCT provided for the first time a high-resolution cross-sectional view through the living retina, comparable to a histological section but without requiring retinal excision. It is important to emphasize that OCT did not just provide an increase in resolution; it literally provided a view of the living retina that was previously completely inaccessible. This feature and the fact that it is a relatively robust technology helped it gain the widespread use it enjoys today.

The idea had been around since the early 1970s that one might recover the depth profile of thick tissue from the variation in the time it takes for light to return from different depths. But the speed of light is so high that this is not practical to measure, and the early pioneers of OCT seized instead on low coherence interferometry. The historical roots of low coherence interferometry lay in the observation by Hooke (1664) that interference could be observed between two reflective surfaces illuminated in white light. This phenomenon was later analyzed by Isaac Newton, and became known as "Newton's rings". The basic principle of marshalling low coherence to measure depth profiles in the eye is shown in Fig. 4A, in the context of what is now called time domain OCT. A light source is used that has very short coherence length, ideally small compared with the retinal layers one wishes to distinguish. This short coherence length implies that when the beam is split in two by a fiber coupler and one beam is directed at the retina and the second one to a reference mirror, the two beams, when brought back together, can only interfere if the two beams traveled the same optical path length to within the coherence length of the source. Shifting the axial position of the reference mirror changes the depth in the retina where interference can be produced, and the magnitude of the interference signal at that depth increases with the intensity of the reflection. By measuring the magnitude of the interference signal as a function of the axial position of the reference mirror, it is possible to identify the light reflected from
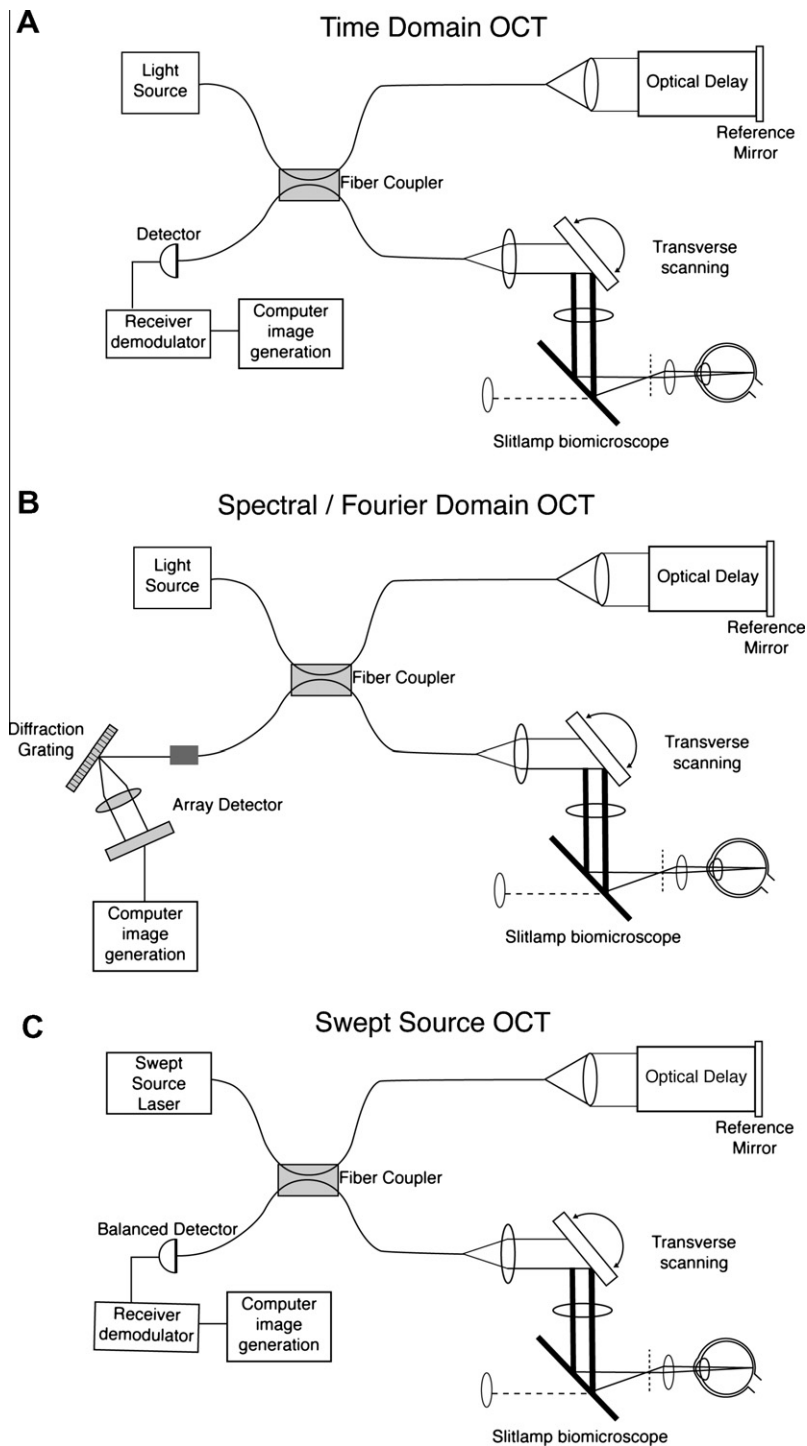
Fig. 4. Three methods that use low coherence interferometry to acquire high resolution depth information from the retina. (A) Time domain OCT. (B) Spectral or Fourier domain OCT. (C) Swept source OCT. See text for details. Adapted from Fujimoto (2003).

different depths, without the need to measure the transit time of light. The earliest application of these ideas to the eye produced a depth profile along a line passing through a single point on the retina, allowing, for example, very precise measurements of the axial length of the eye (e.g. Fercher et al., 1988). By transverse scanning, sequentially acquiring axial depth profiles along a linear series of locations across the retina, one can construct a two-dimensional tomograph or retinal cross-section in the living eye. OCT is able to detect much weaker signals from the retina than conventional fundus imaging because it takes advantage of the in-

creased gain provided by heterodyne detection. In heterodyne detection, the amplitude of the interference signal is proportional to the product of the amplitudes of the two interfering beams so that the use of a large amplitude reference beam amplifies the weak interference signal. Huang and colleagues, working in Jim Fujimoto's laboratory at MIT, made the first in vitro optical coherence tomograph of the retina in 1991 (Huang et al., 1991). Fercher's group made the first in vivo optical coherence tomography of the optic disc in 1993 (Fercher, Hitzenberger, Drexler, Kamp, & Sattmann, 1993).

The next major step in the evolution of OCT was to improve the axial resolution even further. The first systems had a fairly long coherence length, which provided a theoretical resolution of about 10–15 μm. In 1999, Drexler, working in Jim Fujimoto's lab, pioneered the use of broader band, shorter coherence length, sources that could in principle achieve an axial resolution of 3 μm in the eye, two orders of magnitude better than the confocal SLO (Drexler et al., 1999). Though the resolution improvement is limited to a single spatial dimension, ultrahigh resolution OCT could in theory produce a point spread function in the axial dimension smaller than the size of many cells in the retina.

A major limitation of time-domain OCT is the speed at which the retina can be scanned. This is especially problematic because large movements of the eyes could occur even with the fastest scanning speeds available. The main limitation on the speed of image acquisition in time domain OCT is the time required to shift the optical path length in the reference arm of the interferometer, either through mechanical displacement of the mirror or a variable delay line. Avoiding this delay, Fercher introduced the basic principle of spectral domain OCT (Fercher, Hitzenberger, Kamp & El-Zaiat, 1995). A typical layout for a spectral domain OCT is shown in Fig. 4B. It is similar to the time domain OCT with the exception of the detection arm of the system, which contains a spectrometer instead of a simple light detector. The spectrometer consists of a diffraction grating and a one-dimensional CCD that can acquire the entire spectrum of the light returning from a single retinal location in parallel. Spectral domain OCT obviates the need for scanning in the reference arm to acquire the depth profile at each retinal location. Instead, the reflectance at each depth is obtained from variations in the pattern of interference across the spectrum of the reflected light. The spectrum contains depth information because the light reflected from a single depth at one retinal location will generally produce a sinusoidal variation in the interference pattern across wavelength. The amplitude of this sinusoid is proportional to the square root of the amplitude of the electric field reflected at that point. The frequency of this sinusoid increases as the optical path length difference between the reference and sample increases. Therefore, the Fourier transform of the spectrum of the light returning from reflection will reveal the amount of light reflected at each axial depth at that retinal location. The first demonstration of its application in retinal imaging was published in 2002 (Wojtkowski, Kowalczyk, Leitgeb, & Fercher, 2002; Wojtkowski,

Leitgeb, Kowalczyk, Bajraszewski, & Fercher, 2002). The introduction of spectral domain OCT (sometimes called Fourier or frequency domain OCT) increased the sensitivity of OCT by roughly two orders of magnitude. The reason for this improvement is because, in time-domain OCT, at any instant, all the light is lost that is illuminating other retinal layers than the one that happens to be interfering with the reference arm. In spectral domain OCT, at any instant, light from all retinal layers contribute to defining the axial profile. An example of a spectral domain OCT scan from Werner's group at UC, Davis is shown in Fig. 5.

Swept source OCT is a related method that also generates the depth profile through spectral information. In swept source OCT, the wavelength of the light source is rapidly swept to obtain the necessary spectral information to compute the depth profile at each retinal location (Choma, Sarunic, Yang, & Izatt, 2003). The layout of a swept source OCT system is shown in Fig. 4C. Many groups are now acquiring three-dimensional volumes of the retina with these methods (e.g. Drexler & Fujimoto, 2008). These evolving technologies have revolutionized retinal imaging in ophthalmology and two decades after the introduction of the first time domain OCT systems, they are ubiquitous tools in the eye clinic. Though OCT offers a 100-fold improvement in axial resolution over the confocal SLO and is even better still in that dimension than the conventional fundus camera, it does not improve provide any resolution gains in either of the other two lateral spatial dimensions. Fortunately, a way to improve lateral resolution was also under development in the 1990s.

5. Improvements in lateral resolution through adaptive optics

The quality of fundus cameras is typically good enough that the lateral resolution is limited not by the instrument but by the optical quality of the human eye. The limitations in eyes with relatively good optics include diffraction by the eye's pupil and aberrations, with light scatter becoming a significant source of blur in older eyes and young eyes with unusually cloudy optics. The effects of diffraction and aberrations on the eye's point spread function are illustrated in Fig. 6. When both diffraction and aberrations are present, the optimum pupil diameter is in the range of 2–3 mm. If diffraction were the only source of image blur, then for microscopic imaging there would be a clear advantage of using the larg-
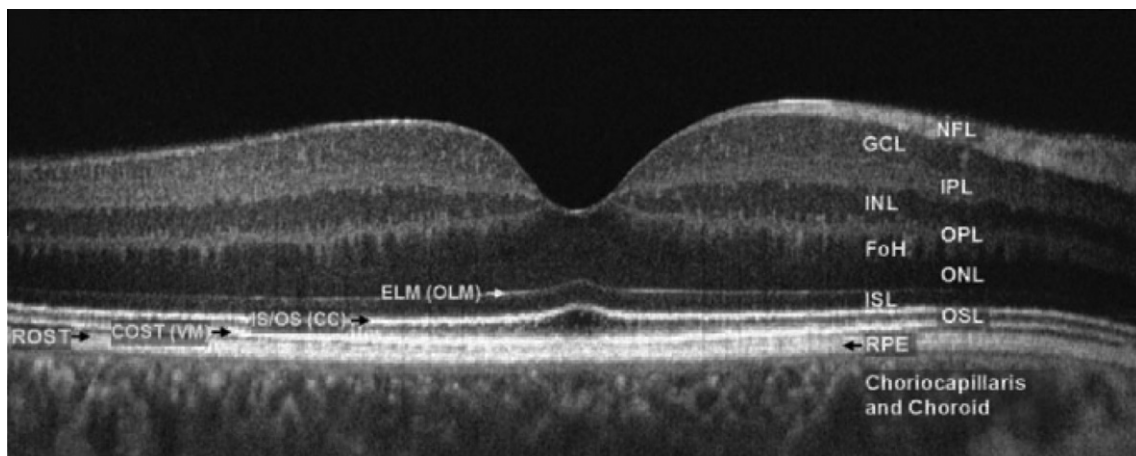
Fig. 5. Fourier-domain optical coherence tomography (FD-OCT) B-scan of the fovea from a normal 34-year-old volunteer acquired with a FD-OCT instrument scanning 5 mm laterally. The instrument was built by Jack Werner's group at UC, Davis. Abbreviations: FoH, fibers of Henle; GCL, ganglion cell layer; INL, inner nuclear layer; IPL, inner plexiform layer; ISL, inner segment layer; NFL, nerve fiber layer; ONL, outer nuclear layer; OPL, outer plexiform layer; OSL, outer segment layer; RPE, retinal pigment epithelium, choriocapillaris and choroid. The outer limiting membrane (OLM; sometimes called external limiting membrane (ELM)), connecting cilia (CC; sometimes called inner/outer segment junction), Verhoeff's membrane (VM; sometimes called cone photoreceptor outer segment tips (COST)) and rod photoreceptor outer segment tips (ROST) may also be seen. ROST and RPE appear as one layer in the fovea but are visible as separate layers in the periphery. From Werner, Keltner, Zawadzki, and Choi (2011).

Fig. 6. The point spread function (PSF) for a diffraction-limited eye and a normal eye at two different pupil diameters. The PSF corresponds to the light distribution on the retina produced by a point source of light infinitely distant from the eye. For the hypothetical diffraction-limited eye, the PSF diameter decreases in inverse propo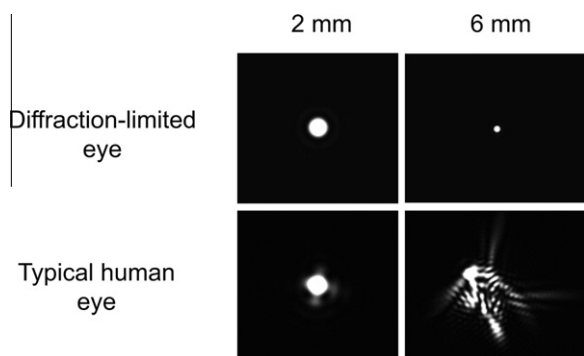rtion to the pupil diameter such that large pupils produce the best image quality. However, in the typical human eye, aberrations increase with increasing pupil size, eliminating the benefit of escaping diffraction at the largest pupils. The goal of AO is to correct the aberrations to produce the PSF of a diffraction-limited eye with a large pupil. From Yin and Williams (2011).

est pupil possible. In theory, retinal imaging without any aberrations and a pupil fully dilated to 8 mm could produce a point spread function with a full width at half height as small as 1.4 μm in the middle of the visible spectrum. Unfortunately, in the typical eye, aberrations corrupt the point spread function at large pupil diameters, removing most of the benefit of escaping diffraction. Full aberration correction with an 8 mm pupil could provide a 3.4-fold gain in lateral resolution over that obtained with a 2.5 mm entrance pupil. This benefit applies to two spatial dimensions, reducing the 3-d volume of the PSF by a factor of ~10. This benefit in lateral resolution does not include the potential benefit in axial resolution that can be achieved by correcting aberrations to be discussed later.

In conventional fundus cameras designed for wide field clinical imaging, no attention is usually paid to correcting aberrations other than defocus. But if the goal is to maximize the lateral resolution of microscopes for imaging the living retina at a cellular spatial scale, it is necessary to compensate not only for defocus, but also astigmatism and a host of other aberrations that we now refer to as higher order aberrations. A quarter of a century ago, higher order aberrations were collectively called "irregular astigmatism". Only a few devoted disciples of physiological optics had succeeded in characterizing some of the individual aberrations that make up irregular astigmatism, and because no method existed to correct them, the importance of their work went largely unrecognized. Smirnov (1961) used a subjective vernier task to measure the third- and fourth-order aberrations of the eye. He lamented the lengthy calculations required to compute the wave aberration and stated that it was unlikely this method would have practical significance, not foreseeing the rapid increase in computing speed that would make it possible within 40 years to measure and compute the eye's wave aberration in a few tens of milliseconds. Walsh, Charman, and Howland (1984) demonstrated the first objective method to measure the eye's wave aberration. This was a significant breakthrough in the history of aberration measurement, but the method was never widely adopted because it was never automated.

Liang, working as a graduate student in Josef Bille's laboratory at the University of Heidelberg demonstrated that it was possible to adapt for use in the eye the Shack–Hartmann wavefront sensor that is widely used in astronomical adaptive optics (Liang et al., 1994). Liang joined my laboratory at the University of Rochester to develop a high-resolution wavefront sensor that provided a more complete description of the eye's wave aberration, measuring up to 10 radial Zernike orders (Liang & Williams, 1997). The

Shack–Hartmann wavefront sensor was eventually automated in a collaborative effort between Artal's group at the University of Murcia and my group at Rochester (Hofer, Artal, Singer, Aragon, & Williams, 2001; Hofer, Chen, et al., 2001). The automation of wavefront sensing and the promise of correcting higher order aberrations with laser refractive surgery lead to rapid commercialization. Even though some of the eye's higher order aberrations had been measured in various clever ways for more than 40 years, their significance for vision correction and high resolution retinal imaging was not widely recognized until adaptive optics was used successfully to correct them.

6. Early adaptive optics systems for the eye

The wave aberration is unique in every eye and it is dynamic over time, largely due to fluctuations in focus (Hofer, Artal, et al., 2001; Hofer, Chen, et al., 2001). Therefore, the correction of the wave aberration requires an optical element that could assume an essentially infinite number of possible shapes over time. Fortunately, just such a technology had been developed to solve a related problem in the field of astronomy. The idea of adaptive optics was first introduced by Babcock (1953), who suggested that an adaptive optical element could remove the blur in stellar images from the time-varying aberrations produced by the turbulent atmosphere. Babcock was unable to implement his idea at the time because the technology did not exist to measure and correct the aberrations he could see dancing just out of reach in the pupil plane of his telescope. Hardy and his colleagues succeeded in the first empirical demonstration of adaptive optics in astronomy (Hardy, Lefebvre, & Koliopoulos, 1977). Now adaptive optics is commonplace among the best ground-based telescopes around the world.

In 1989, Dreher, working in Joseph Bille's laboratory at the University of Heidelberg, used a deformable mirror to improve retinal
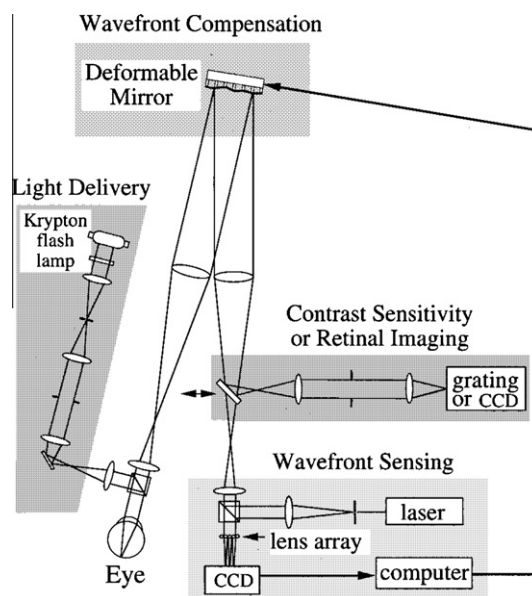
Fig. 7. Optical layout of the first adaptive optics fundus camera that could correct higher order aberrations of the human eye. *Wave-front sensing and adaptive compensation.* The eye focused a collimated laser beam onto the retina. The light reflected from the retina formed an aberrated wave front at the pupil. The distorted wave front was measured by a Hartmann–Shack wave-front sensor. A deformable mirror, conjugate with the pupil, compensated for the eye's wave aberration. After compensation was achieved, psychophysical or retinal imaging experiments could be performed with a 6-mm pupil. *Retinal imaging.* A krypton flash lamp delivered a 4-ms flash, illuminating a retinal disk 1° in diameter. A scientific-grade CCD acquired images of the retina. From Liang et al. (1997).

images in a scanning laser ophthalmoscope (Dreher, Bille, & Weinreb, 1989), correcting the astigmatism in one subject's eye based on a conventional spectacle prescription. At the time, Bille's group had not yet developed the Shack–Hartmann wavefront sensor, so that they were not able to correct additional aberrations beyond astigmatism.

Liang, Miller, and I constructed the first closed-loop adaptive optics system that could correct higher order aberrations in the eye, shown in Fig. 7 (Liang, Williams, & Miller, 1997). The system consisted of a Shack–Hartmann wavefront sensor to measure the eye's aberrations, a 37 actuator deformable mirror to correct the aberrations, and a flash-illuminated fundus camera to acquire a retinal image once the eye's aberrations had been compensated through the AO control loop. This first system required about 15 min for each loop of measuring and correcting the wave aberration, with 4 or 5 loops required to complete the correction. As slow as this system was, it could produce better images of the cone mosaic than Miller had previously obtained without adaptive optics. Real time, automated adaptive optics systems soon followed (Fernandez, Iglesias, & Artal, 2001; Hofer, Chen, et al., 2001).

7. Color vision and the trichromatic cone mosaic

Shortly after the AO fundus camera was developed, it was applied to the problem of imaging the trichromatic organization of the cone mosaic in the human retina. Though it had been known for nearly 200 years that human color vision relies on three channels each tuned to a different part of the visible spectrum

(Young, 1801), the arrangement and relative numbers of all three cone classes in the human eye had not been subject to direct scrutiny. Roorda, then a postdoc at the University of Rochester, combined retinal densitometry (Campbell & Rushton, 1955) with adaptive optics, making it possible to reliably identify the photopigment in single cones throughout large patches of cones near the foveal center (Roorda, Metha, Lennie, & Williams, 2001; Roorda & Williams, 1999).

The signal to noise ratio of single images of the cone mosaic was too poor to reliably identify the pigment contained in each cone. This made it necessary to add many images. Eye movements that occurred between frames are typically many times larger than the diameter of a cone, so that it was necessary to register multiple frames with cross-correlation before adding them. This approach turned out to be effective at increasing signal-to-noise ratio without compromising image quality through registration error. Putnam et al. (2005) later showed that it is possible to record the retinal location of a fixation target on discrete trials with an error at least five times smaller than the diameter of the smallest foveal cones. These results showed how accurate this process could be, and that registration error with high quality AO images can be smaller than the point spread function of the aberration corrected image. The ability to register and add such high spatial resolution images turns out to be key to microscopic retinal imaging because safety limits often preclude delivering all the light in a single exposure.

The results of Roorda's analysis, and subsequent measurements by Hofer, Carroll, Neitz, Neitz, and Williams (2005) showed that
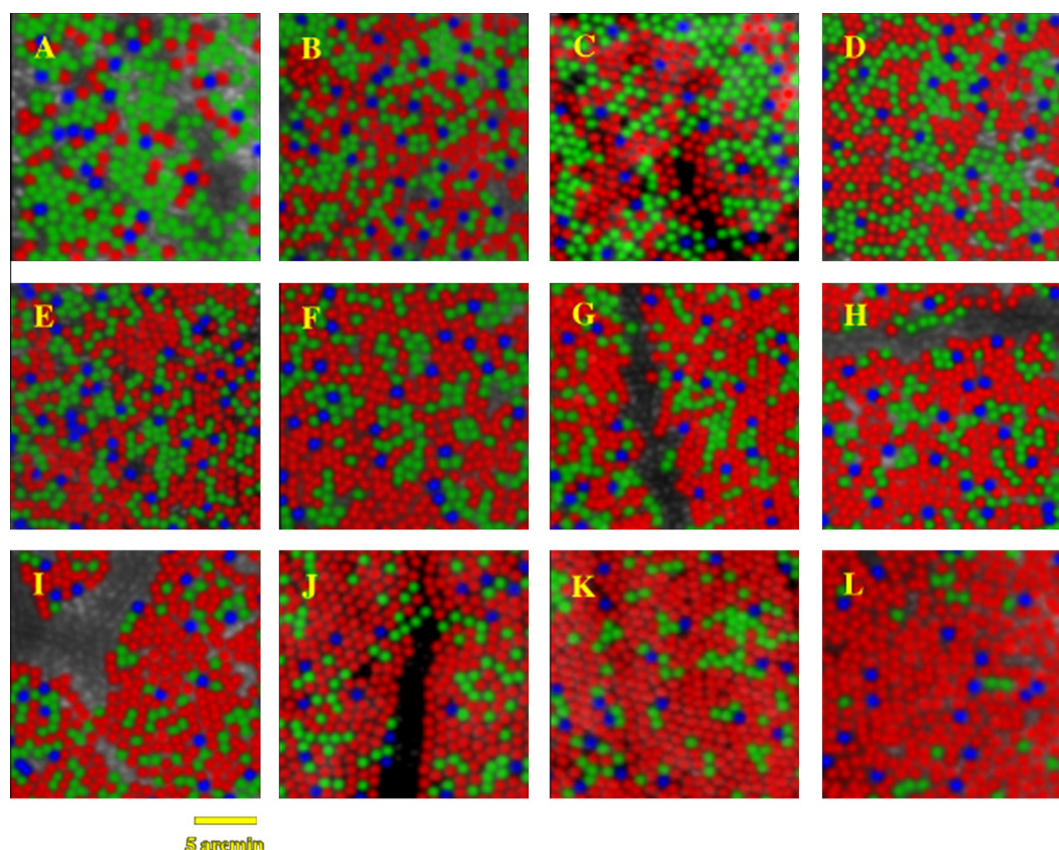
Fig. 8. Images of the cone mosaics of 10 subjects with normal color vision, obtained with the combined methods of adaptive optics imaging and retinal densitometry. The images are false colored so that blue, green, and red are used to represent the S, M, and L cones respectively. (The true colors of these cones are yellow, purple, and bluish-purple.) The mosaics illustrate the enormous variability in L/M cone ratio. The L/M cone ratios are A, 0.37, B, 1.11, C, 1.14, D, 1.24, E, 1.77, F, 1.88, G, 2.32, H, 2.36, I, 2.46, J, 3.67, K, 3.90, L, 16.54. The proportion of S cones is relatively constant across eyes, ranging from 3.9% to 6.6% of the total population. Images were taken either 1° or 1.25° from the foveal center. For two of the 10 subjects, two different retinal locations are shown. Panels D and E show images from nasal and temporal retinas respectively for one subject; J and K show images from nasal and temporal retinas for another subject. Images C, J, and K are from Roorda and Williams (1999). All other images are from Hofer et al. (2005). From Williams and Hofer (2003).

Fig. 9. AO reveals cone mosaics in two kinds of color blindness. (a) Dichromat with cone mosaic indistinguishable from a normal trichromat. (b) Dichromat with M pigment 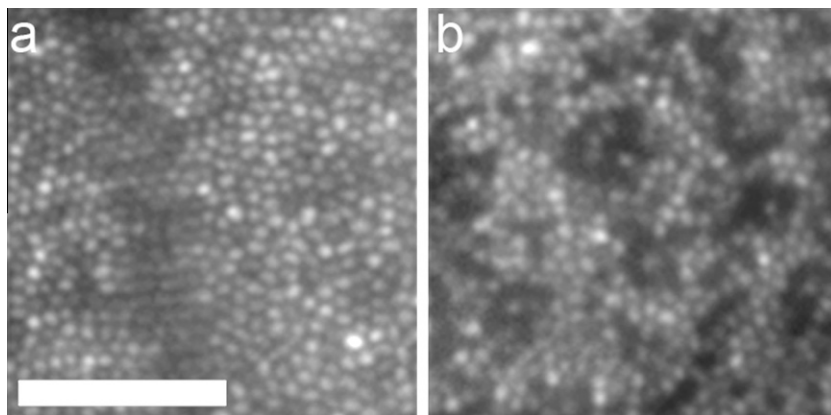mutation showing dark regions where cones may be damaged or lost; despite the disruption in the cone mosaic this person has excellent spatial vision. Scale is identical for each panel; scale bar is 50 μm. From Carroll et al. (2004).

the distribution of the different photopigments in foveal cones is essentially random and revealed directly a very large (40-fold) variation in the relative numbers of L and M cones across individuals (see Fig. 8). One of the most powerful aspects of the ability to characterize the trichromatic mosaic in the living human eye is that it allows psychophysical measures of visual performance that can be directly correlated with mosaic organization. For example, it allowed experiments that demonstrate that color experience is not affected by the relative numbers of L and M cones (Brainard et al., 2000; Neitz, Carroll, Yamauchi, Neitz, & Williams, 2002).

8. Adaptive optics for vision correction

Adaptive optics corrects the wave aberration simultaneously for light entering the eye as well as light leaving the eye. This makes it useful both for vision correction and for retinal imaging. By way of example, it has also allowed experiments in which flashes smaller than single photoreceptors are delivered to the cone mosaic to probe the color experience produced when single cones are stimulated (Hofer, Singer, & Williams, 2005). These experiments showed that cones containing the same photopigment do not always generate the same color appearance, supporting the view that color appearance depends also on the identities of nearby cones (Brainard, Williams, & Hofer, 2008).

The use of adaptive optics for vision correction has expanded in many exciting new directions, not only for studying vision when aberrations are corrected (e.g. Artal, Manzanera, Piers, & Weeber, 2010; Atchison, Guo, Charman, & Fisher, 2009; Atchison, Guo, & Fisher, 2009; Dalimier & Dainty, 2008; Dalimier, Dainty, & Barbur, 2008; de Gracia et al., 2010; Elliott et al., 2009; Guo & Atchison, 2010; Gupta, Guo, Atchison, & Zele, 2010; Li, Xiong, Li, et al., 2009; Li, Xiong, Wang, et al., 2009; Liang et al., 1997; Lundstrom et al., 2007; Marcos, Sawides, Gambra, & Dorronsoro, 2008; Perez, Manzanera, & Artal, 2009; Rocha, Vabre, Chateau, & Krueger, 2010; Rocha, Vabre, Harms, Chateau, & Krueger, 2007; Rossi & Roorda, 2010; Rossi, Weiser, Tarrant, & Roorda, 2007; Rouger, Benard, & Legras, 2009; Sawides, Gambra, Pascual, Dorronsoro, & Marcos, 2010; Williams et al., 2000; Yoon & Williams, 2002). Adaptive optics can be used to study visual performance by generating specific novel aberration patterns in the eye (e.g. Chen, Singer, Guirao, Porter, & Williams, 2005). This use of adaptive optics has revealed that the nervous system has adapted to the specific pattern of aberrations in the eye (Artal et al., 2003; Atchison & Guo, 2010; Chen, Artal, Gutierrez, & Williams, 2007; Sabesan & Yoon, 2010). AO vision correction systems have also been used to study other

aspects of vision such as motion processing (Raghunandan, Frasier, Poonja, Roorda, & Stevenson, 2008), accommodation (Chen, Kruger, Hofer, Singer, & Williams, 2006; Fernandez & Artal, 2005; Hampson, Chin, & Mallen, 2010), and binocular vision (Fernández, Prieto, & Artal, 2010). AO may ultimately provide a rapid and highly reliable alternative to the subjective phoropter used to refract the eye.

9. Genetics and the cone mosaic

Another advantage of in vivo resolution of the human photoreceptor mosaic is that it made it vastly simpler to determine how polymorphisms in the genes that code for the photoreceptors influence the mosaic that is ultimately formed. Carroll and colleagues (Carroll, Neitz, Hofer, Neitz, & Williams, 2004), working initially on the flood-illuminated AO ophthalmoscope at Rochester discovered a new cause for color blindness in which a mutation in the gene for one of the three cone photopigments results in a mosaic of cones that shows patchy loss (see Fig. 9). Interestingly, despite the loss of nearly 1/3 of the patient's foveal cones, his visual acuity is normal (20/15), indicating that adaptive optics imaging can detect retinal degeneration well before conventional clinical tests. Carroll and colleagues have gone onto describe the mosaic phenotype of an impressive number of different polymorphisms (Baraas et al., 2007; Carroll et al., 2009, 2010; Wagner-Schuman et al., 2010).

10. Adaptive optics scanning laser ophthalmoscopy

The adaptive optics fundus camera built at the University of Rochester had a greatly improved lateral resolution over cameras without AO but it had effectively no axial sectioning, which meant that scattered light throughout the eye and instrument could reduce image contrast (see Fig. 3). But even the confocal SLOs of the 1980s had a axial sectioning capable of removing corneal and lenticular scatter though, at about ~300 μm, not enough to provide much useful optical sectioning of the retina.

Roorda, then at the University of Houston, and his colleagues built the first instrument that combined the benefits of adaptive optics with those of the confocal SLO (Roorda et al., 2002). The optical layout of an AOSLO is shown in Fig. 10. This new instrument had a number of important advantages. First, adaptive optics increased confocality by increasing the quality of the retinal image at the pinhole, allowing the use of smaller pinholes and therefore better rejection of light from unwanted planes away
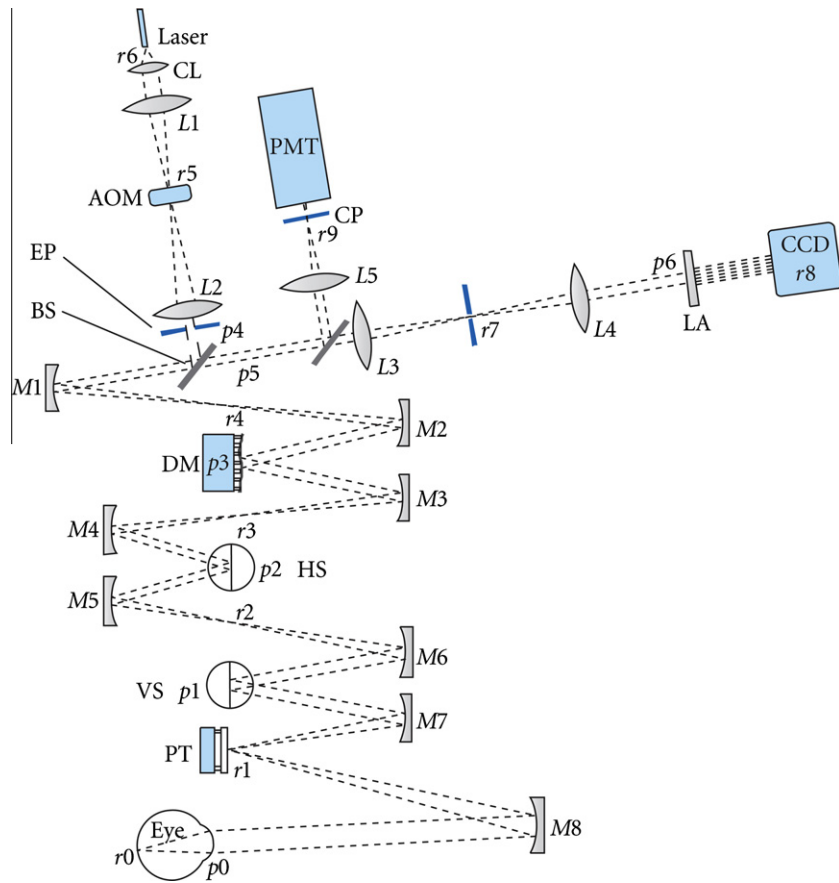
Fig. 10. Schematic of an adaptive optics scanning laser ophthalmoscope invented by Austin Roorda. Key: CL, collimating lens; AOM, acousto-optic modulator; EP, entrance pupil; BS1, beamsplitter 1; DM, deformable mirror; HS, horizontal scanning mirror; VS, vertical scanning mirror; PT, pupil tracking mirror; LA, lenslet array; CP, confocal pinhole; PMT, photomultiplier tube. Pupil and retinal conjugates are labeled p and r, respectively. Mirrors and lenses are labeled M# and L# along the optical path. Telescope lens/mirror-pairs for relaying the pupil through the path are L1–L2, L3–L4, M1–M2, M3–M4, M5–M6, and M7–M8. From Miller and Roorda (2009).

from the image plane. The sectioning capability of the AOSLO is shown in Fig. 11 (see also, Fig. 3). In the most recent AOSLOs at the University of Rochester, this has improved the axial resolution of the first confocal SLOs by about an order of magnitude. Second, the AOSLO provides microscopic resolution with a real-time view of the retina. This has enabled the video-rate imaging of the motion of individual blood cells in the smallest capillaries in the retina (Martin & Roorda, 2005, 2009; Zhong, Petrig, Qi, & Burns, 2008; Zhong, Song, Chui, Petrig, & Burns, in press). Tam, Martin, and Roorda (2010) has improved the imaging of retinal vasculature without the need for fluorescein by using motion contrast to identify vessels, setting the stage for automated measurements of leukocyte velocity (Tam, Tiruveedhula, & Roorda, 2011). In vivo studies of blood flow in these smallest of vessels may provide valuable information about early vascular changes in diseases such as diabetic retinopathy.

The clinical utility of AO imaging is only now beginning to be explored (Baraas et al., 2007; Bhatt, Rha, Carroll, & Stepien, 2010; Carroll et al., 2004, 2009, 2010; Chen, Roorda, & Duncan, 2010; Choi et al., 2006; Hammer et al., 2008; McAllister et al., 2010; Talcott et al., 2010; Wolfing, Chung, Carroll, Roorda, & Williams, 2006; Yoon et al., 2009). An exciting recent paper has also shown the potential of AO in drug development (Talcott et al., 2011). They have shown that the AOSLO can detect photoreceptor rescue by a drug, CNTF, in retinitis pigmentosa patients. The value of AO is highlighted by the fact that other standard clinical measures such as visual acuity failed to show a benefit. It seems likely that the microscopic views of cells provided by AO will find their place in

the clinic as an especially sensitive indicator of the progression of retinal disease.

In scanning systems such as the SLO, eye movements produce distortion within individual frames as well as translation between frames. The AOSLO is also subject to these distortions, but the increased resolution AO affords allows us to resolve the effects of eye movements at a finer spatial scale. Roorda and collaborators (Stevenson & Roorda, 2005; Vogel, Arathorn, Roorda, & Parker, 2006) have shown that they can use the warping that occurs in individual frames and between frames in their AOSLO to recover what is probably the most accurate measurement of eye motion ever made. Methods to track the retina with an accuracy approaching the dimensions of single cells will become increasingly important in obtaining enough signal to distinguish subtle changes in retinal cells. Stabilization of the field of view would be especially useful in situations such as microsurgery performed with a microscope equipped with adaptive optics. It is now possible to perform these computations in real time, allowing real-time stabilization of the retinal image for targeted delivery of visual stimuli to the retina (Arathorn et al., 2007; Yang, Arathorn, Tiruveedhula, Vogel, & Roorda, 2010). An alternative approach, under development by Ferguson and Hammer at Physical Sciences Corporation and Burns at Indiana University, is to couple a separate eye tracker to an adaptive optics scanning laser ophthalmoscope for the purposes of image stabilization (Burns, Tumbar, Elsner, Ferguson, & Hammer, 2007; Hammer et al., 2006). Hybrid systems that combine hardware tracking and software stabilization are also under development.
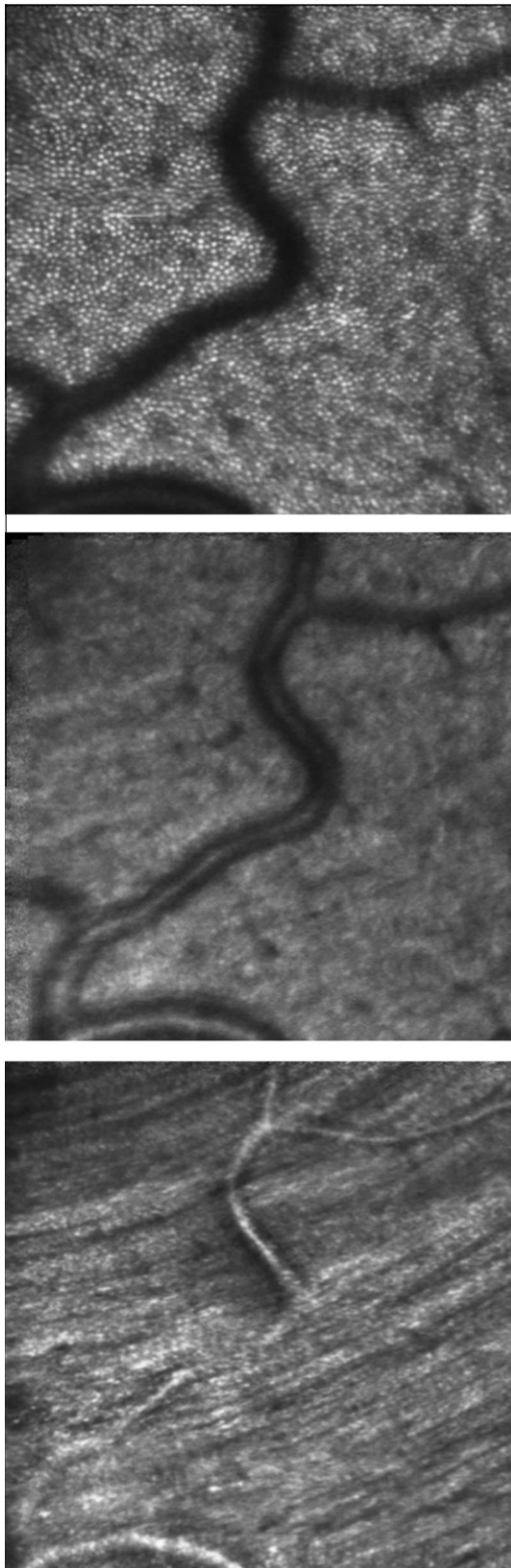
Fig. 11. Optical sectioning of the retinal layers. In the top panel, the AOSLO is focused at the external limiting membrane and shows the mosaic of cone photoreceptors. The middle panel is an optical section of the inner retina, showing light scattered from the blood vessels. The bottom panel is an optical section with the focus on the surface of the retina, showing the striation of the nerve fiber bundles. The image is from a location about 4° inferior to the foveal center. From Roorda (2010).
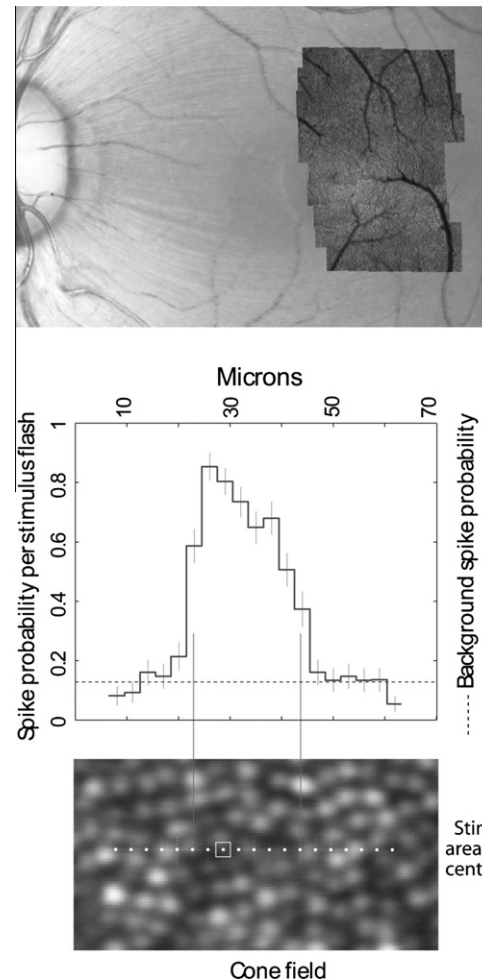

Fig. 12. Mapping single cone cell inputs to the receptive fields of LGN cells recorded with a microelectrode in the monkey. Upper panel: color fundus photograph of macaque retina with an AOSLO montage overlay. The red dot indicates the location of the receptive field that is shown in the two lower panels. The lower panel shows the exact locations of the test areas. The central plot shows the probability that each stimulus flash will produce a neural spike (adapted from Sincich et al. (2009)). From Roorda (2010).

11. Single unit physiology and single cone inputs to LGN receptive fields

These approaches may herald a new generation of psychophysical experiments in which the location of a stimulus on the retinal cone mosaic can be controlled in real time with an error less than the diameter of a single cone. Indeed, Sincich and colleagues (Sincich, Zhang, Tiruveedhula, Horton, & Roorda, 2009) have shown that the AOSLO can be combined with single unit electrical recordings of spike trains in primate lateral geniculate nucleus. Remarkably, as shown in Fig. 12, through exquisite control a point source delivered with AO despite eye movements, they have been able to target and stimulate single cones, recording the responses of LGN cells to light arriving in single cones. This method will ultimately allow the microdissection of the cone inputs to receptive fields of cells at many stages in the visual pathway in the intact organism.

12. Imaging the smallest photoreceptors

The performance of adaptive optics systems is steadily improving due to the use of better designs that minimize instrument
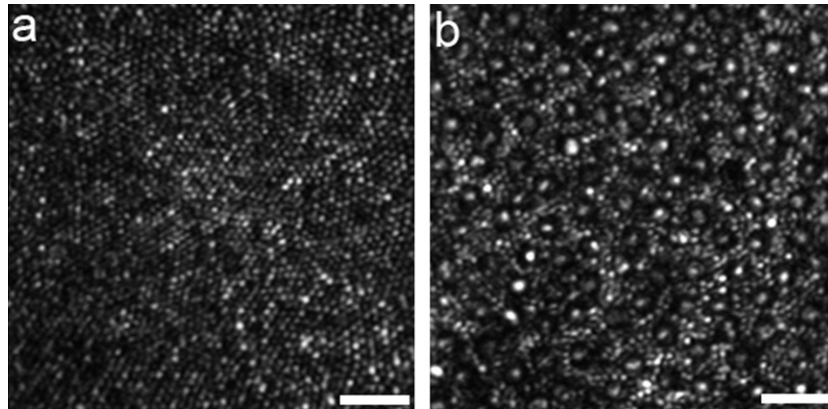
Fig. 13. High-resolution images of the smallest photoreceptors obtained with the new Rochester AOSLO. (a) The complete foveal cone mosaic. (b) The complete peripheral photoreceptor mosaic showing both rods and cones, imaged at 101 temporal and 11 inferior. Scale bars are 20 μm. From Rossi et al. (2011).

aberrations (Dubra & Sulai, in press; Gomez-Vieyra, Dubra, Mala-cara-Hernandez, & Williams, 2009), the use of smaller confocal pinholes, and improvements in registration algorithms. Fig. 13a shows an image obtained with Alfredo Dubra's AOSLO at the University of Rochester, in which the smallest cones at the foveal center can be resolved. Building on the earlier work of Carroll, Choi, and Williams (2008), Doble et al. (2011), and Dubra et al. (in press) can now obtain clear images of single rods in the living human eye (Fig. 13b). Rods are much more difficult than cones to resolve because of their small diameter (~2 μm) and broad angular tuning, which sends less light back through the pupil where it can be collected for imaging. The ability to image rods routinely would be valuable in assessing the progression of retinal degeneration, which often begins with an assault on the rods.

13. High resolution fluorescence imaging

The introduction of fluorescein angiography revealed the enormous potential of fluorescence retinal imaging for improving the contrast of specific retinal features. The first use of fluorescence in the living human eye was in 1960, when MacLeand and Maumenee used a slit lamp to directly view intravenously-injected fluorescein in the eye (MacLean & Maumenee, 1960). The following year, Novotny and Alvis (1961) combined this method with a fundus camera, collecting the first fluorescein angiograms. Indocyanine green angiography, which provides an enhanced view of blood flow in the choroids was introduced in 1969 (David, 1969).

A quarter century ago, these were essentially the only fluorescence methods available in the living eye, but the use of fluorescence has since expanded. An especially exciting example of the resurgence in interest in fluorescence is the recent demonstration of in vivo fluorescence SLO imaging of apoptosis of single primate ganglion cells stained with annexin-5 (Cordeiro, Guo, Luong, et al., 2004). It may someday be possible to track cells on the path to apoptosis in humans with glaucoma. The high contrast provided by fluorescence when only occasional cells are labeled plus the relatively large size of ganglion cells make it easy to resolve these cells without resorting to high resolution methods. Surprisingly, the mouse eye, with a numerical aperture twice that of the human, has a theoretical PSF volume that is 16 times smaller than that of the diffraction-limited human eye. Indeed excellent images of ganglion cells have been obtained in the mouse retina without the need for adaptive optics (Leung et al., 2008; Pacques et al., 2006; Seeliger et al., 2005; Walsh & Quigley, 2008). Melissa Geng at the University of Rochester has recently constructed an AOSLO specifically for the mouse eye, having overcome difficulties in wavefront sensing the mouse optics caused by reflections from multiple retinal layers (Geng et al., 2011). This new instrument promises to reveal subcellular features in the mouse retina never before accessible in the living eye.

Another major new direction in fluorescence imaging began in 1995 when von Ruckmann introduced lipofuscin autofluorescence imaging (von Ruckmann, Fitzke, & Bird, 1995). Lipofuscin is comprised of a number of compounds that are by-products of the visual cycle of photopigment bleaching and regeneration. They
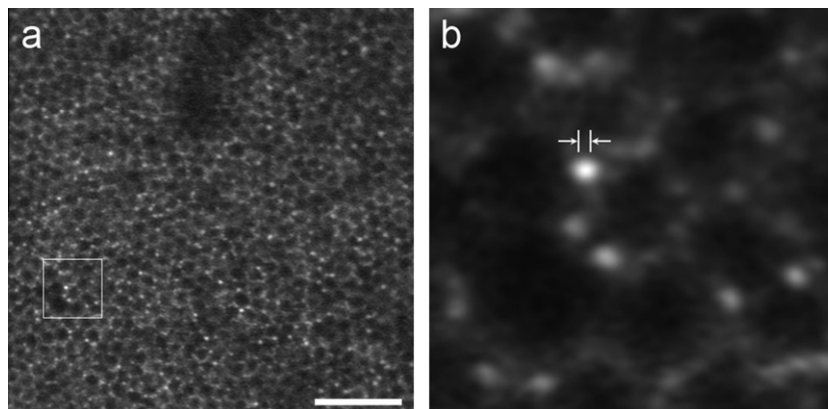

Fig. 14. Retinal pigment epithelium and individual lipofuscin granules revealed in FAOSLO. (a) Individual RPE cells imaged using FAOSLO in macaque. Scale bar is 100 μm. (b) Outlined region from a showing individual lipofuscin granules; distance between arrowheads is 2 μm, on the order of the size expected for RPE granules. From Rossi et al. (2011).

accumulate throughout life and are autofluorescent, making it possible to image the retinal pigment epithelium (RPE) for the first time in the living eye. The retinal pigment epithelium lies just behind the photoreceptors and is critically important in servicing them. RPE cells are replete with melanin granules, one role of which is to absorb light that would otherwise scatter and compromise the contrast of the retinal image. But a consequence of this protective role of melanin is that the RPE cells have relatively low contrast and are difficult to image with reflected light in the living eye (but see Roorda, Zhang, & Duncan, 2007). Autofluorescence imaging was quickly incorporated in commercial instruments, allowing an entirely new view of retinal diseases that compromise the RPE layer.

14. Imaging RPE cells and ganglion cells with a fluorescence AOSLO

Commercial autofluorescence imaging is achieved with flood-illuminated fundus cameras or confocal SLOs equipped with the appropriate blocking filters. Building on the AOSLO technology introduced by Roorda and colleagues, Gray, Morgan and others at the University of Rochester added fluorescence imaging capabilities, making it possible to image single RPE cells in the living primate eye (see Fig. 14). The FAOSLO has provided the first in vivo images of the RPE cell mosaic in the normal primate eye (Gray et al., 2006; Morgan, Dubra, Wolfe, Merigan, & Williams, 2009), taking advantage of the resolution provided by adaptive optics and the AF of lipofuscin inside RPE cells. In a typical frame, the signal measured by the PMT corresponds to only 0.2 photons/pixel, so over a thousand frames are typically averaged to generate an image. Eye motion between successive frames requires image registration before averaging, but the images are too dim to self-register. To overcome this problem, the FAOSLO simultaneously records a high signal–noise-ratio (SNR) movie of the photoreceptors using reflectance imaging in the near infrared and a low SNR fluorescence movie of the RPE in the visible. Since the two movies share the same retinal motion, cross-correlation of cone frames can be used to compute the eye motion correction for the dimmer RPE frames. Discrete RPE cells can be seen because the cell nucleus does not contain lipofuscin and appears dark, whereas the cytoplasm surrounding the nucleus appears bright due to lipofuscin AF.

As shown in Fig. 15, Gray has also shown that it is possible to image ganglion cells including subcellular features such as their dendrites (Gray et al., 2008). The rapid development of fluorescent probes in biology and medicine as well as new methods, such as viral-based methods, to deliver these probes promises to revolutionize retinal imaging. It may soon be possible to image stimulus dependent changes in ganglion cell fluorescence through genetically encoded calcium indicators in the living eye (see Borghuis et al. (2011) for an in vitro demonstration of this approach), which

could ultimately clarify why the retina requires 17 or more distinct ganglion cell pathways to convey the retinal image to the brain. To date, in vivo cellular microscopic imaging methods are largely confined to animal imaging, and a major hurdle for the future is to find noninvasive methods to exploit these fluorophores in human retinal imaging.

15. A point spread function equal to 3 μm in all three spatial dimensions

It was recognized soon after adaptive optics was first demonstrated in the eye that its high lateral resolution would complement the ultrahigh axial resolution of OCT. By combining the two technologies in a single instrument, the point spread function can be approximately 3 μm (see Fig. 3). Miller et al. (2011) has recently reviewed the current state of AO-OCT. Miller and his colleagues were the first to combine AO and an en face coherence gated camera, achieving an axial resolution of 14 μm and a lateral resolution of 3–5 μm (Miller, Qu, Jonnal, & Thorn, 2003). Shortly thereafter, Artal's group at the University of Murcia, Spain and Drexler's group at the University of Vienna collaborated to produce the first generation AO UHR OCT using time domain detection (Hermann et al., 2004). Since then there has been a striking proliferation of AO-OCT instruments based on many different types of OCT systems including time domain en face scanning (Merino, Dainty, Bradu, & Podoleanu, 2006; Pircher, Zawadzki, Evans, Werner, & Hitzenberger, 2008), high resolution spectral domain OCT (Bigelow et al., 2007; Zawadzki, Choi, Jones, Oliver, & Werner, 2007; Zawadzki et al., 2005; Zhang, Rha, Jonnal, & Miller, 2005; Zhang et al., 2006), ultra-high spectral domain OCT (Cense et al., 2009; Fernandez et al., 2005, 2008; Kocaoglu et al., 2011;Torti et al., 2009; Zawadzki et al., 2008), and swept source OCT (Mujat et al., 2010).

There are a number of challenges in the successful marriage of AO and OCT. One of these is the need to correct the eye's longitudinal chromatic aberration because of the large spectral bandwidth required for high resolution OCT. The axial resolution of OCT, as mentioned earlier, is inversely proportional to the spectral bandwidth of the source. Ultrahigh resolution OCT demands sufficiently large bandwidths that chromatic aberration can significantly reduce image quality (Fernandez & Drexler, 2005; Fernandez et al., 2006). Not only does AO-OCT increase the lateral resolution up to five times over commercial OCT, by employing a larger pupil, it reduces the grain of speckle and increases the sensitivity of the instrument to light reflected out of the eye. AO-OCT systems have be used to image a number of retinal structures such as individual nerve bundles in the nerve fiber layer (Cense et al., 2009; Torti et al., 2009; Zawadzki et al., 2008), the smallest capillaries around the rim of the foveal avascular zone, (Hammer et al., 2008; Wang et al., in press) as well as single cone photoreceptors (Cense
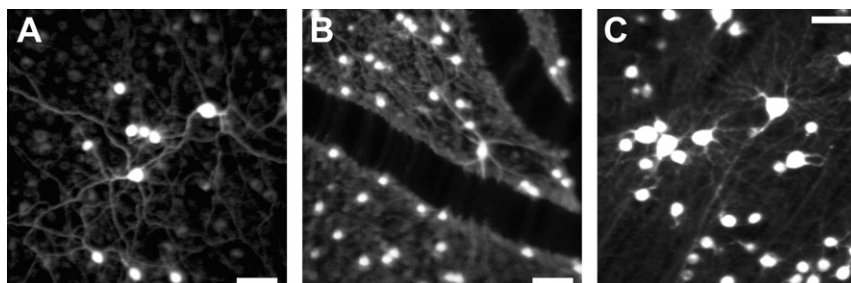
Fig. 15. Fluorescence AOSLO images of primate retinal ganglion cells in vivo. (A–C) Fluorescence AOSLO imaging revealed the morphology of retinal ganglion cells labeled with fluorophore (rhodamine dextran) in living monkey eye. The transverse resolution of the images is fine enough to resolve the individual dendrites. The fluorophore was introduced into the ganglion cells through retrograde labeling via injections in the lateral geniculate nucleus (LGN). Scale bar of 50 μm in all panels. [Panels A and C, reproduced from Gray et al. (2008), their Figs. 1 and 5, with permission from Association for Research in Vision and Ophthalmology (Copyright 2008).]

Fig. 16. AO-OCT volume acquired over a 1° retinal region located temporal of the fovea, as illustrated by the rectangle in the fundus photograph. The images on the right are en face views of particular retinal layers extracted from the AO-OCT volume. Retinal layers from top to bottom are: nerve fiber layer (NFL), ganglion cell layer (GCL), outer plexiform layer (OPL), and outer segment layer of photoreceptors (OS). From Miller et al. (2011).

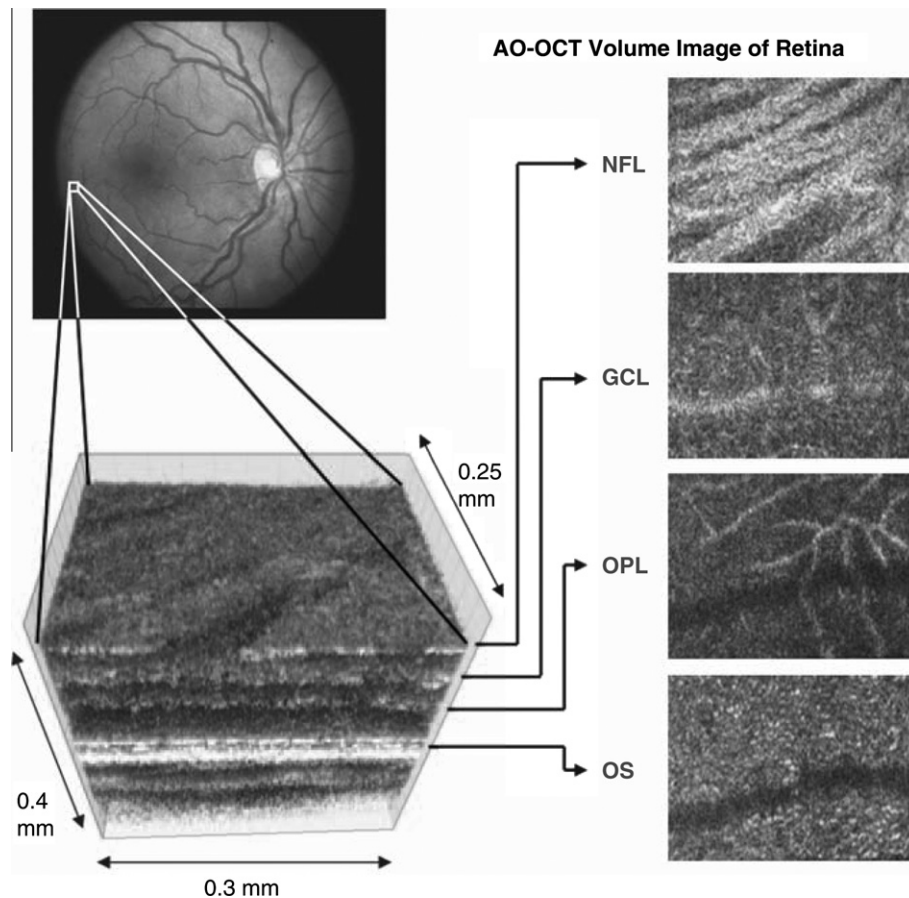et al., 2009; Fernandez et al., 2008; Torti et al., 2009; Zawadzki et al., 2007, 2008; Zhang et al., 2006). It also has been deployed to study several diseases of the eye such as retinopathy of prematurity (Hammer et al., 2008) and optic neuropathies (Choi, Zawadzki, Keltner, & Werner, 2008; Choi et al., 2011). Fig. 16 shows an examples of a 3-D volumetric reconstruction of the retina from an AO-OCT system.

16. Functional changes in single cones with adaptive optics interferometry

Miller and his group at Indiana University have undertaken a series of very elegant experiments on single cones in the living human eye that beautifully illustrate the scientific potential of adaptive optics coupled with low coherence interferometry (Jonnal et al., 2007, 2010). While AO-OCT usually involves the use of a scanning engine and a point detector, in some cases it is possible to combine AO and low coherence interferometry to great advantage in a CCD-based flash-illuminated camera. Their flash-illuminated AO system can acquire images of cones with a high-speed CCD at rates as high as 192 Hz, ~1000 times faster than the first flood-illuminated AO ophthalmoscope he helped to build at the University of Rochester. Conveniently, most of the light reflected from cones comes from just two layers corresponding to the two ends of the cone outer segment, at the inner/outer segment junction and at the junction between the outer segment and the underlying RPE cell (see Fig. 17). Miller's instrument illuminates the cone mosaic with light of low coherence length but high enough that light reflected from these two layers within each single cone can

interfere. This clever arrangement converts each cone into a living, single cell interferometer that is exquisitely sensitive to very subtle changes in optical path length within the cone. Because this interferometer, unlike most other OCT methods, has both the reference and sample beams inside the photoreceptor, it is insensitive to external vibration and motion that can plague interferometers that have separate paths for the reference and sample. Miller's group has shown for the first time that they can record an optical path length change within photoreceptors that begins within 5–10 ms of visual stimulation of a cone. Moreover, as shown in Fig. 18 they can also record the slow growth of each cone outer segment, which is only about 100 nm/h! This process of the outer segment renewal is thought to be critical for the photoreceptor to continue to transduce light into an electrical signal and has never been resolved in vivo before. Under these specialized conditions, this instrument has the best depth resolution ever demonstrated in the eye, and can detect changes in outer segment length as small as 140 nm, more than 20 times better than the theoretical axial resolution of ultra-high resolution optical coherence tomography, and more than a 1000-fold better than the confocal scanning laser ophthalmoscope.

17. Looking forward

Aside from the satisfaction of basking in our progress, there seems to be little point in dwelling on the past unless it guides us in the future. One lesson from dwelling on the past is that the major improvements in retinal imaging technology throughout history have sprung from advances in other fields, especially
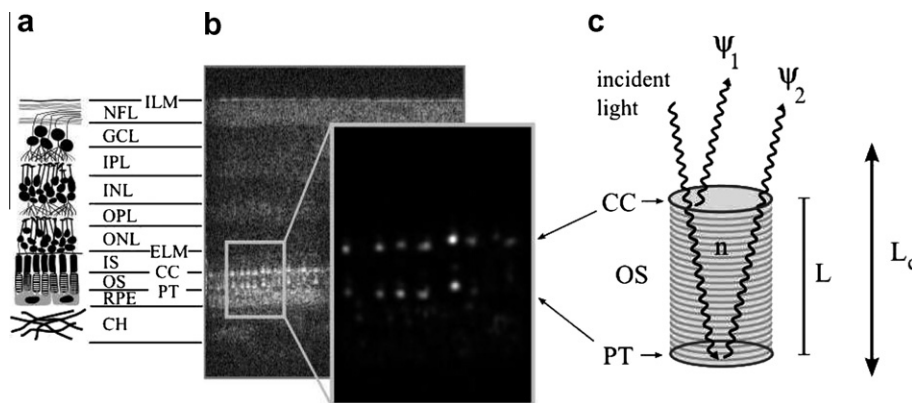
Fig. 17. The reflective structure of the retina showing the two bright reflections especially from the cone photoreceptors that are the basis for cellular interferometry. (a) A diagram depicting the major layers of the neural retina, consisting of the inner limiting membrane (ILM), nerve fiber layer (NFL), ganglion cell layer (GCL), inner plexiform layer (IPL), inner nuclear layer (INL), outer plexiform layer (OPL), outer nuclear layer (ONL), external limiting membrane (ELM), the inner segments (IS) and outer segments (OS) (which make up the photoreceptor layer), the connecting cilia (CC) and posterior tip (PT) layers (which bound the outer segment), the retinal pigment epithelium (RPE), and the choroid (CH). (b) An AO-OCT B-scan (log intensity), showing a cross-section of the full retinal thickness, aligned with the layers depicted in (a), and an enlarged view (linear intensity) of the cone outer segments. While OCT images are typically shown in log intensity, the linear intensity view of the outer segments demonstrates vividly that the bulk of the cone reflection originates at the CC and PT layers: the bright, patterned reflections at the CC and PT layers are the most visible structures in the linear intensity image; their peak intensity is more than two orders of magnitude greater than the average intensity of all other layers in the image. Each distinct reflection in the pattern represents a single cone cell. (c) A model of light propagation through the OS. Two bright reflections (Ψ_1 and Ψ_2) originate from the CC and PT layers, creating a biological interferometer in the retina that is sensitive to small ($\ll \lambda$) changes in the outer segment length L whenever the temporal coherence length of the illumination source L^c is longer than L. From Jonnal et al. (2010).

optics, microscopy, and astronomy. This repeats a pattern that has pervaded the history of vision science and ophthalmology at least as early as Kepler, an astronomer who first stated unequivocally in 1604 that the retinal image is inverted. Others from the physical sciences who have made seminal contributions to vision science and ophthalmology include Helmholtz, Herschel, Maxwell, Newton, Schiener, and Young to name just a few. It is especially interesting how long it takes for significant technical advances in other fields to migrate into the eye. Confocal imaging, OCT, and adaptive optics were all introduced in other domains decades before they were applied to the eye. Part of this delay has to do with the lack of availability or high cost of the hardware required to implement new technologies; I will never forget the $1M price tag on the only deformable mirror available when I first contemplated building an adaptive optics ophthalmoscope at the University of Rochester. The demonstration of closed loop adaptive optics for the eye had to wait until the price tag dropped more than an order of magnitude. It also takes time to learn a new technology and to implement the modifications required to make it work in the eye. Another delay may be the result of scientific provincialism and insularity, a delay that could be reduced by increased scrutiny of the latest developments in those fields that have historically fueled ophthalmoscopy. On the bright side, if history is any guide, the next major breakthrough in retinal imaging technology was almost certainly made decades ago and is just waiting for an enterprising scientist or engineer to translate it into the eye.

The developers of new technology for retinal imaging may be unaware that they have something in common with cave divers. Both enjoy an extreme sport that is more often than not an exercise in the management of claustrophobia. The cave diver's view of his cramped world is of almost entirely impenetrable rock. The developer of retinal imaging technology is similarly boxed in by the fundamental limits of physics and biology. Both grope along, driven by the hope of discovering a previously-missed passage that, if they can just squeeze through, will open up into whole new possibilities for exploration. The history of retinal imaging would suggest, however, that fundamental limits are rarely if ever fundamental limits of the natural world. They are almost always fundamental limits of the conceptual framework we have chosen to think in. The conventional wisdom in 1990 held that axial resolution was fundamen-

tally constrained by geometrical optics and depth of focus. But by adding the wave properties of light to the conceptual framework, practitioners of low coherence interferometry in the eye surprised everyone with a 100-fold, and now recently a 1000-fold, improvement in axial resolution over what was thought possible before.

Though it is true that the speed of light has stood its ground as a fundamental limit for a very long time, can we really say with confidence that any limits are truly impenetrable? Progress in high-resolution retinal imaging demands that we treat these limits as invitations to overcome them. It may seem that the spectral transmittance of the cornea and lens would pose a fundamental limit on noninvasive optical imaging of the retina, forever preventing us from interrogating molecules that absorb light only in spectral regions outside the ocular transmittance window. But as illustrated in Fig. 19, Hunter and colleagues have recently shown that two-photon imaging can excite autofluorescent molecules in the living retina that have excitation spectra in the near UV, outside the spectral pass band of the eye's optics (Hunter et al., 2011). If this method can be made more efficient, it could open up an entirely new way to study retinal structure and function in the living eye.

Another major constraint on microscopic retinal imaging is the maximum permissible light exposure that can be delivered without damaging the eye. This constraint is especially troublesome given that the typical yield in reflectance imaging is one photon back for every 10,000 that enter the pupil. The problem is compounded by the high magnification that microscopic retinal imaging demands, as well as the low efficiency of many potentially informative light-tissue interactions. But the dramatic improvements in eye tracking described earlier make it possible to maintain high spatial resolution and avoid thermal light damage by harvesting light at reduced power over longer times. Moreover, compounds have been discovered that protect the eye from photochemical light damage (e.g. Maeda et al., 2006), and the application of these prior to imaging could make it possible to observe faint retinal signals that are presently invisible. In addition, we are at the beginning of a revolution in the availability of contrast enhancing fluorophores that one can direct to particular classes of retinal neurons with increasing specificity, functional imaging capabilities, and improved quantum efficiency.
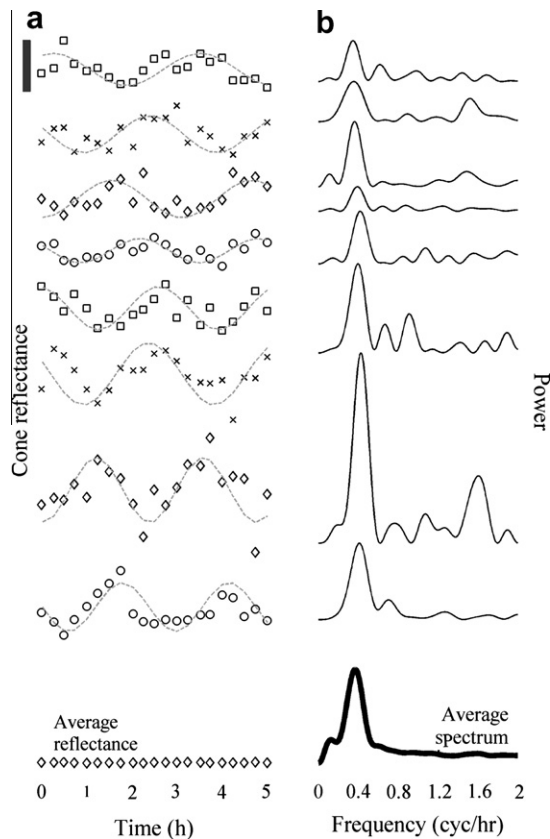
Fig. 18. Cone reflectances and their power spectra (plots offset vertically for ease of viewing). (a) Reflectance as a function of time of eight sample cones taken from trial 4. Superimposed on each plot is a cosine fit (gray line). The black bar in the upper left shows 1/10th of the average DC component, I_0, of cone reflectance. The oscillation of reflectance in all cones had a visible period of 2.5–3 h, while the amplitudes and phases appeared to vary randomly. At the bottom is a plot of the average reflectance of all cones (diamonds), nearly flat (contrast 0.18%), which is predicted by the model shown in Fig. 1c and Eq. (1). (b) Power spectra of mean-subtracted cone reflectance traces shown in a, and the average spectrum of all 1626 cones (dark line). Most cones in this trial had a visible peak in the power spectrum around 0.37 cyc/h, and this peak is visible in the average power spectrum as well. Similar peaks were seen in power spectra of individual cones, and the average power spectrum, in all trials in which the long coherence source was used (these frequencies are summarized in Table 1). When the short coherence source was used, neither the power spectra of individual cones nor the average power spectrum showed comparable peaks. From Jonnal et al. (2010).

The diffraction limit is another fundamental barrier that is just now coming under scrutiny in the domain of retinal microscopy (Shroff, Fienup, & Williams, 2009; Shroff, Fienup, & Williams, 2010). Abbe (1837) showed nearly 140 years ago that the wave nature of light poses a fundamental barrier on the resolution of an optical system with a fixed numerical aperture. If the diffraction limit could be surpassed, then a new leap to smaller spatial scales in retinal imaging would be enabled, scales that in principle could be molecular. Most scientists and engineers long ago resigned themselves to the notion that the diffraction limit was so fundamental to the nature of light that it would never be surpassed in any practical imaging system. Remarkably, the field of microscopy has already seen the diffraction barrier fall, not once but many times, thanks to an array of new techniques including structured illumination (Gustafsson, 1999), stimulated emission depletion (Hell & Wichmann, 1994), and photoactivation localization microscopy (Betzig et al., 2006). None of these methods has yet been applied successfully to retinal imaging, and certainly the challenges of doing so are formidable. But the history of the past quarter century strongly suggests that new routes around fundamental barriers will be found, allowing us to acquire ever more information from the living retina.

Conflict of interest

My employer, the University of Rochester, holds intellectual property on which I am an inventor and that pertain to the subject matter of this article.

Acknowledgments

References

Arathorn, D. W., Yang, Q., Vogel, C. R., Zhang, Y., Tiruveedhula, P., & Roorda, A. (2007). Retinally stabilized cone-targeted stimulus delivery. *Optics Express, 15*, 13731–13744.
Artal, P., Chen, L., Fernandez, E. J., Singer, B., Manzanera, S., & Williams, D. R. (2003). Adaptive optics for vision: The eye's adaptation to point spread function. *Journal of Refractive Surgery, 19*(5), S585–S587.

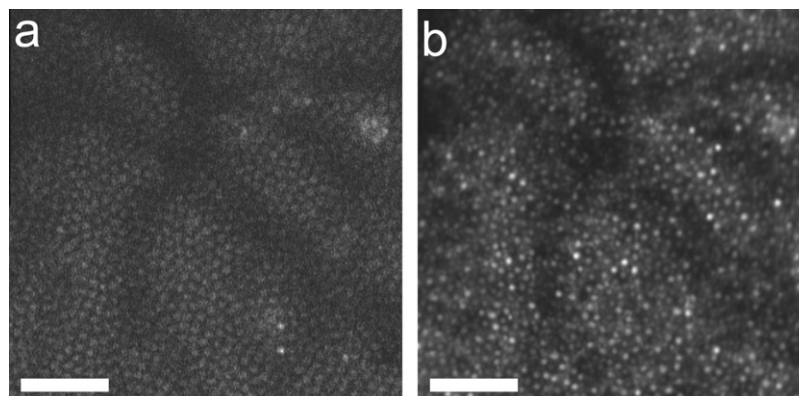**Fig. 19.** (A) two-photon image of the cone mosaic in the living primate retina at 2.5° superior retina using 730 nm illumination from a Ti-Sapph laser with a pulse width of less than 70 fs. (B) Reflectance image of the cone mosaic at the same location using 790 nm light. The bright spots in both images correspond, confirming the cone mosaic as the origin of the two photon signal. Scale bar, 50 μm.

Artal, P., Manzanera, S., Piers, P., & Weeber, H. (2010). Visual effect of the combined correction of spherical and longitudinal chromatic aberrations. *Optics Express, 18*(2), 1637–1648.

Artal, P., & Navarro, R. (1989). High-resolution imaging of the living human fovea: Measurement of the intercenter cone distance by speckle interferometry. *Optics Letters, 14*, 1098–1100.

Atchison, D. A., Guo, H., Charman, W. N., & Fisher, S. W. (2009). Blur limits for defocus, astigmatism and trefoil. *Vision Research, 49*(19), 2393–2403.

Atchison, D. A., Guo, H., & Fisher, S. W. (2009). Limits of spherical blur determined with an adaptive optics mirror. *Ophthalmic and Physiological Optics, 29*(3), 300–311.

Atchison, D. A., & Guo, H. (2010). Subjective blur limits for higher order aberrations. *Optometry and Vision Science, 87*(11), E890–E898.

Babcock, H. W. (1953). The possibility of compensating astronomical seeing. *Publications of the Astronomical Society of the Pacific, 65*, 229–236.

Baraas, R. C., Carroll, J., Gunther, K. L., Chung, M., Williams, D. R., Foster, D. H., et al. (2007). Adaptive optics retinal imaging reveals S-cone dystrophy in tritan color-vision deficiency. *Journal of the Optical Society of America A – Optics Image Science and Vision, 24*(5), 1438–1447.

Betzig, E., Patterson, G. H., Sougrat, R., Lindwasser, O. W., Olenych, S., et al. (2006). Imaging intracellular fluorescent proteins at nanometer resolution. *Science, 313*, 1642–1645.

Bhatt, S. S., Rha, J., Carroll, J., & Stepien, K. (2010). Imaging photoreceptor structure in punctate inner choroidopathy using adaptive optics ophthalmoscopy and spectral domain optical coherence tomography. *Investigative Ophthalmology and Visual Science, 51* (E-abstract 2332).

Bigelow, C. E., Iftimia, N. V., Ferguson, R. D., Ustun, T. E., Bloom, B., & Hammer, D. X. (2007). Compact multimodal adaptive-optics spectral-domain optical coherence tomography instrument for retinal imaging. *Journal of the Optical Society of America A – Optics Image Science and Vision, 24*(5), 1327–1336.

Borghuis, B. G., Tian, L., Xu, Y., Nikonov, S. S., Vardi, N., Zemelman, B. V., et al. (2011). Imaging light responses of targeted neuron populations in the rodent retina. *Journal of Neuroscience, 31*(8), 2855–2867.

Brainard, D. H., Roorda, A., Yamauchi, Y., Calderone, H. B., Metha, A., Neitz, M., et al. (2000). Functional consequences of the relative numbers of L and M cones. *Journal of the Optical Society of America A – Optics Image Science and Vision, 17*, 607–614.

Brainard, D., Williams, D. R., & Hofer, H. (2008). Trichromatic reconstruction from the interleaved cone mosaic: Bayesian model and the color appearance of small spots. *Journal of Vision, 8*(5), 1–23.

Burns, S. A., Tumbar, R., Elsner, A. E., Ferguson, D., & Hammer, D. X. (2007). Large-field-of-view, modular, stabilized, adaptive-optics-based scanning laser ophthalmoscope. *Journal of the Optical Society of America A – Optics Image Science and Vision, 24*(5), 1313–1326.

Campbell, F. W., & Rushton, W. A. H. (1955). Measurement of the scotopic pigment in the living human eye. *Journal of Physiology, 130*, 131–147.

Carroll, J., Baraas, R. C., Wagner-Schuman, M., Rha, J., Siebe, C. A., Sloan, C., et al. (2009). Cone photoreceptor mosaic disruption associated with Cys203Arg mutation in the M-cone opsin. *Proceedings of the National Academy of Sciences of the United States of America, 106*(49), 20948–20953.

Carroll, J., Choi, S. S., & Williams, D. R. (2008). In vivo imaging of the photoreceptor mosaic of a rod monochromat. *Vision Research, 48*(26), 2564–2568.

Carroll, J., Neitz, M., Hofer, H., Neitz, J., & Williams, D. R. (2004). Functional photoreceptor loss revealed with adaptive optics: An alternate cause of color blindness. *Proceedings of the National Academy of Sciences of the United States of America, 101*(22), 8461–8466.

Carroll, J., Rossi, E. A., Porter, J., Neitz, J., Roorda, A., Williams, D. R., et al. (2010). Deletion of the x-linked opsin gene array locus control region (LCR) results in disruption of the cone mosaic. *Vision Research, 50*(19), 1989–1999.

Cense, B., Koperda, E., Brown, J. M., Kocaoglu, O. P., Gao, W., Jonnal, R. S., et al. (2009). Volumetric retinal imaging with ultrahigh-resolution spectral-domain optical coherence tomography and adaptive optics using two broadband light sources. *Optics Express, 17*(5), 4095–4111.

Chen, L., Artal, P., Gutierrez, D., & Williams, D. R. (2007). Neural compensation for the best aberration correction. *Journal of vision, 7*(10), 1–9 (article 9).

Chen, L., Kruger, P. B., Hofer, H., Singer, B., & Williams, D. R. (2006). Accommodation with higher-order monochromatic aberrations corrected with adaptive optics. *Journal of the Optical Society of America A – Optics Image Science and Vision, 23*(1), 1–8.

Chen, L., Singer, B., Guirao, A., Porter, J., & Williams, D. R. (2005). Image metrics for predicting subjective image quality. *Optometry and Vision Science, 82*(5), 358–369.

Chen, Y., Roorda, A., & Duncan, J. L. (2010). Advances in imaging of Stargardt disease. *Advances in Experimental Medicine and Biology, 664*, 333–340.

Choi, S. S., Doble, N., Hardy, J. L., Jones, S. M., Keltner, J. L., Olivier, S. S., et al. (2006). In vivo imaging of the photoreceptor mosaic in retinal dystrophies and correlations with visual function. *Investigative Ophthalmology and Visual Science, 47*, 2080–2092.

Choi, S. S., Zawadzki, R. J., Keltner, J. L., & Werner, J. S. (2008). Changes in cellular structures revealed by ultra-high resolution retinal imaging in optic neuropathies. *Investigative Ophthalmology and Visual Science, 49*(5), 2103–2119.

Choi, S. S., Zawadzki, R. J., Lim, M. C., Brandt, J. D., Keltner, J. L., Doble, N., et al. (2011). Evidence of outer retinal changes in glaucoma patients as revealed by ultrahigh-resolution in vivo retinal imaging. *British Journal of Ophthalmology, 95*(1), 131–141.

Choma, M., Sarunic, M., Yang, C., & Izatt, J. (2003). Sensitivity advantage of swept source and Fourier domain optical coherence tomography. *Optics Express, 11*(18), 2183–2189.

Cideciyan, A. V., & Jacob, S. G. (1994). Image analysis of the tapetal-like reflex in carriers of X-linked retinitis pigmentosa. *Investigative Ophthalmology and Visual Science, 35*, 3812–3824.

Cordeiro, M. F., Guo, L., Luong, V., et al. (2004). Real-time imaging of single nerve cell apoptosis in retinal neurodegeneration. *Proceedings of the National Academy of Sciences of the United States of America, 101*, 13352–13356.

Costa, R. A., Skaf, M., Melo, L. A., Jr., Calucci, D., Cardillo, J. A., Castro, J. C., et al. (2006). Retinal assessment using optical coherence tomography. *Progress in Retinal and Eye Research, 25*(3), 325–353 (review).

Dalimier, E., & Dainty, C. (2008). Use of a customized vision model to analyze the effects of higher-order ocular aberrations and neural filtering on contrast threshold performance. *Journal of the Optical Society of America A – Optics Image Science and Vision, 25*(8), 2078–2087.

Dalimier, E., Dainty, C., & Barbur, J. L. (2008). Effects of higher-order aberrations on functional vision as a function of light level. *Journal of Modern Optics, 55*, 791–803.

David, N. J. (1969). Infrared absorption fundus angiography. In *Proceedings from the International Symposium on Fluorescein Angiography, Albi.* Basel: Karger; 1971; 198–192.

de Gracia, P., Dorronsoro, C., Gambra, E., Marin, G., Hernandez, M., & Marcos, S. (2010). Combining coma with astigmatism can improve retinal image over astigmatism alone. *Vision Research, 50*(19), 2008–2014.

Doble, N., Choi, S. S., Codona, J. L., Christou, J., Enoch, J. M., & Williams, D. R. (2011). In vivo imaging of the human rod photoreceptor mosaic. *Optics Letters, 36*(1), 31–33. doi:10.1364/OL.36.000031.

Dreher, A. W., Bille, J. F., & Weinreb, R. N. (1989). Active optical depth resolution improvement of the laser tomographic scanner. *Applied Optics, 28*, 804–808.

Drexler, W., & Fujimoto, J. G. (2008). State-of-the-art retinal optical coherence tomography. *Progress in Retinal and Eye Research, 27*(1), 45–88 (review).

Drexler, W., Morgner, U., Kartner, F. X., Pitris, C., Boppart, S. A., Li, X. D., et al. (1999). In vivo ultrahigh-resolution optical coherence tomography. *Optics Letters, 24*(17), 1221–1223.

Dubra, A., & Sulai, Y. (in press). The reflective afocal broadband adaptive optics scanning ophthalmoscope. *Biomedical Optics Express*.

Dubra, A., Sulai, Y., Norris, J. L., Cooper, R. F., Dubis, A. M., Williams, D. R., et al. (in press). Non-invasive in vivo imaging of the human rod photoreceptor mosaic using a confocal adaptive optics scanning ophthalmoscope. *Biomedical Optics Express*.

Elliott, S. L., Choi, S. S., Doble, N., Hardy, J. L., Evans, J. W., & Werner, J. S. (2009). Role of high-order aberrations in senescent changes in spatial vision. *Journal of Vision, 9*(2), 1–16 (article 24).

Fercher, A. F., Hitzenberger, C. K., Drexler, W., Kamp, G., & Sattmann, H. (1993). In vivo optical coherence tomography. *American Journal of Ophthalmology, 116*(1), 113–114.

Fercher, A. F., Hitzenberger, C. K., Kamp, G., & El-Zaiat, S. Y. (1995). Measurement of intraocular distances by backscattering spectral interferometry. *Optics Communications, 117*, 43–48.

Fercher, A. F., Mengedoht, K., & Werner, W. (1988). Eye-length measurement by interferometry with partially coherent light. *Optics Letters, 13*(3), 186–188.

Fernandez, E. J., & Artal, P. (2005). Study on the effects of monochromatic aberrations in the accommodation response by using adaptive optics. *Journal of the Optical Society of America A – Optics Image Science and Vision, 22*(9), 1732–1738.

Fernandez, E., & Drexler, W. (2005). Influence of ocular chromatic aberration and pupil size on transverse resolution in ophthalmic adaptive optics optical coherence tomography. *Optics Express, 13*(20), 8184–8197.

Fernandez, E. J., Povazay, B., Hermann, B., Unterhuber, A., Sattmann, H., Prieto, P. M., et al. (2005). Three-dimensional adaptive optics ultrahigh-resolution optical coherence tomography using a liquid crystal spatial light modulator. *Vision Research, 45*, 3432–3444.

Fernandez, E. J., Hermann, B., Povazay, B., Unterhuber, A., Sattmann, H., Hofer, B., et al. (2008). Ultrahigh resolution optical coherence tomography and pancorrection for cellular imaging of the living human retina. *Optics Express, 16*(15), 11083–11094.

Fernandez, E. J., Iglesias, I., & Artal, P. (2001). Closed-loop adaptive optics in the human eye. *Optics Letters, 26*(10), 746–748.

Fernández, E. J., Prieto, P. M., & Artal, P. (2010). Adaptive optics binocular visual simulator to study stereopsis in the presence of aberrations. *Journal of the Optical Society of America A – Optics Image Science and Vision, 27*, A48–A55.

Fernandez, E. J., Unterhuber, A., Povazay, B., Hermann, B., Artal, P., & Drexler, W. (2006). Chromatic aberration correction of the human eye for retinal imaging in the near infrared. *Optics Express, 14*(13), 6213–6225.

Fujimoto, J. G. (2003). Optical coherence tomography for ultrahigh resolution in vivo imaging. *Nature Biotechnology, 21*(11), 1361–1367 (review).

Geng, Y., Schery, L., Sharma, R., Dubra, A., Ahmad, K., Libby, R., et al. (2011). Optical properties of the mouse eye. *Biomedical Optics Express, 2*(4), 717–738.

Godara, P., Dubis, A. M., Roorda, A., Duncan, J. L., & Carroll, J. (2010). Adaptive optics retinal imaging: Emerging clinical applications. *Optometry and Vision Science, 87*(12), 930–941.

Gomez-Vieyra, A., Dubra, A., Malacara-Hernandez, D., & Williams, D. R. (2009). First-order design of off-axis reflective ophthalmic adaptive optics systems using afocal telescopes. *Optics Express, 17*(21), 18906–18919.

Gray, D. C., Merigan, W., Wolfing, J. I., Gee, B. P., Porter, J., Dubra, A., et al. (2006). In vivo fluorescence imaging of primate retinal ganglion cells and retinal pigment epithelial cells. *Optics Express, 14*(16), 7144–7158.

Gray, D. C., Wolfe, R., Gee, B. P., Scoles, D., Geng, Y., Masella, B. D., et al. (2008). In vivo imaging of the fine structure of rhodamine-labeled macaque retinal ganglion cells. *Investigative Ophthalmology and Visual Science, 49*(1), 467–473.

Guo, H., & Atchison, D. A. (2010). Subjective blur limits for cylinder. *Optometry and Vision Science, 87*(8), E549–E559.

Gupta, P., Guo, H., Atchison, D. A., & Zele, A. J. (2010). Effect of optical aberrations on the color appearance of small defocused lights. *Journal of the Optical Society of America A – Optics Image Science and Vision, 27*(5), 960–967.

Gustafsson, M. G. L. (1999). Extended resolution fluorescence microscopy. *Current Opinion in Structural Biology, 9*, 627–634.

Hammer, D. X., Ferguson, R. D., Bigelow, C. E., Iftimia, N. V., Ustun, T. E., & Burns, S. A. (2006). Adaptive optics scanning laser ophthalmoscope for stabilized retinal imaging. *Optics Express, 14*(8), 3354–3367.

Hammer, D. X., Iftimia, N. V., Ferguson, R. D., Bigelow, C. E., Ustun, T. E., Barnaby, A. M., et al. (2008). Foveal fine structure in retinopathy of prematurity: An adaptive optics Fourier domain optical coherence tomography study. *Investigative Ophthalmology and Visual Science, 49*(5), 2061–2070.

Hampson, K. M. (2008). Adaptive optics and vision. *Journal of Modern Optics, 55*(21), 3425–3467.

Hampson, K. M., Chin, S. S., & Mallen, E. A. (2010). Effect of temporal location of correction of monochromatic aberrations on the dynamic accommodation response. *Biomedical Optics Express, 1*(3), 879–894.

Hardy, J. W., Lefebvre, J. E., & Koliopoulos, C. L. (1977). Real-time atmospheric compensation. *Journal of the Optical Society of America, 67*, 360–369.

Hecht, S., Schlaer, S., & Pirenne, M. H. (1942). Energy, quanta, and vision. *Journal of General Physiology, 25*, 819–840.

Hell, S. W., & Wichmann, J. (1994). Breaking the diffraction resolution limit by stimulated emission: Stimulated-emission-depletion fluorescence microscopy. *Optics Letters, 19*, 780–782.

Helmholtz, H. L. F. (1851). *Beschreibung eines Augen-Spiegels zur Untersuchung der Netzhaut im lebenden Auge (Description of an eye mirror for the investigation of the retina of the living eye)*. Berlin: A Förstner'sche Verlagsbuchhandlung.

Hermann, B., Fernandez, E. J., Unterhuber, A., Sattmann, H., Fercher, A. F., Drexler, W., et al. (2004). Adaptive-optics ultrahigh-resolution optical coherence tomography. *Optics Letters, 29*(18), 2142–2144.

Hofer, H., Artal, P., Singer, B., Aragon, J. L., & Williams, D. R. (2001). Dynamics of the eye's wave aberration. *Journal of the Optical Society of America A – Optics Image Science and Vision, 18*(3), 497–506.

Hofer, H., Chen, L., Yoon, G. Y., Singer, B., Yamauchi, Y., & Williams, D. R. (2001). Improvement in retinal image quality with dynamic correction of the eye's aberrations. *Optics Express, 8*(11), 631–643.

Hofer, H., Carroll, J., Neitz, J., Neitz, M., & Williams, D. R. (2005). Organization of the human trichromatic cone mosaic. *Journal of Neuroscience, 25*(42), 9669–9679 (Erratum in: Journal of Neuroscience 2006, 26(2), 722).

Hofer, H., Singer, B., & Williams, D. R. (2005). Different sensations from cones with the same photopigment. *Journal of Vision, 5*(5), 444–454.

Hooke, R. (1664). Micrographia: Some physiological descriptions of minute bodies made by magnifying glasses with observations and inquiries thereupon.

Huang, D., Kaiser, P. K., Lowder, C. Y., & Traboulsi, E. I. (2006). *Retinal imaging*. Philadelphia: Elsevier, Inc.

Huang, D., Swanson, E. A., Lin, C. P., Schuman, J. S., Stinson, W. G., Chang, W., et al. (1991). Optical coherence tomography. *Science, 254*(5035), 1178–1181.

Hunter, J., Masella, B., Dubra, A., Sharma, R., Yin, L., Merigan, W., et al. (2011). Images of photoreceptors in living primate eyes using adaptive optics two-photon ophthalmoscopy. *Biomedical Optics Express, 2*(1), 139–148.

Huygens, C. (1678). *Treatise on light*.

Jackman, W. T., & Webster, J. D. (1886). On photographing the retina of the living human eye. *Philadelphia Photographer, 23*, 340–341.

Jagger, W. S. (1985). Visibility of photoreceptors in the intact cane toad eye. *Vision Research, 25*, 729–731.

Jonnal, R. S., Besecker, J. R., Derby, J. C., Kocaoglu, O. P., Cense, B., Gao, W., et al. (2010). Imaging outer segment renewal in living human cone photoreceptors. *Optics Express, 18*(5), 5257–5270. doi:10.1364/OE.18.005257.

Jonnal, R. S., Rha, J., Zhang, Y., Cense, B., Gao, W., & Miller, D. T. (2007). In vivo functional imaging of human cone photoreceptors. *Optics Express, 15*(4), 16141–16160.

Kocaoglu, O. P., Lee, S., Jonnal, R. S., Wang, Q., Herde, A. E., Derby, J. C., et al. (2011). Imaging cone photoreceptors in three dimensions and in time using ultrahigh resolution optical coherence tomography with adaptive optics. *Biomedical Optics Express, 2*(4), 748–763.

Labeyrie, A. (1970). Attainment of diffraction-limited resolution in large telescopes by Fourier-analyzing speckle patterns in star images. *Astronomy and Astrophysics, 6*, 85–87.

Land, M. F., & Snyder, A. W. (1985). Cone mosaic observed directly through natural pupil of live vertebrate. *Vision Research, 25*, 1519–1523.

Leung, C. K., Lindsey, J. D., Growston, J. G., Lijia, C., Chiang, S., & Weinreb, R. N. (2008). Longitudinal profile of retinal ganglion cell damage after optic nerve crush with blue-light confocal scanning laser ophthalmoscopy. *Investigative Ophthalmology and Visual Science, 49*, 4898–4902.

Li, J., Xiong, Y., Wang, N., Li, S., Dai, Y., Xue, L., et al. (2009). Effects of spherical aberration on visual acuity at different contrasts. *Journal of Cataract and Refractive Surgery, 35*(8), 1389–1395.

Li, S., Xiong, Y., Li, J., Wang, N., Dai, Y., Xue, L., et al. (2009). Effects of monochromatic aberration on visual acuity using adaptive optics. *Optometry and Vision Science, 86*(7), 868–874.

Liang, J., Grimm, B., Goelz, S., & Bille, J. F. (1994). Objective measurement of wave aberrations of the human eye with the use of a Hartmann–Shack wavefront sensor. *Journal of the Optical Society of America A – Optics Image Science and Vision, 11*, 1949–1957.

Liang, J., & Williams, D. R. (1997). Aberrations and retinal image quality of the normal human eye. *Journal of the Optical Society of America A – Optics Image Science and Vision, 14*, 2873–2883.

Liang, J., Williams, D. R., & Miller, D. T. (1997). Supernormal vision and high-resolution retinal imaging through adaptive optics. *Journal of the Optical Society of America A – Optics Image Science and Vision, 14*(11), 2884–2892.

Lundstrom, L., Manzanera, S., Prieto, P. M., Ayala, D. B., Gorceix, N., Gustafsson, J., et al. (2007). Effect of optical correction and remaining aberrations on peripheral resolution acuity in the human eye. *Optics Express, 15*(20), 12654–12661.

MacLean, A. L., & Maumenee, A. E. (1960). Hemangioma of the choroid. *Transactions of the American Ophthalmological Society, 50*(1), 3–11.

Maeda, A., Maeda, T., Golczak, M., Imanishi, Y., Leahy, P., Kubota, R., et al. (2006). Effects of potent inhibitors of the retinoid cycle on visual function and photoreceptor protection from light damage in mice. *Molecular Pharmacology, 70*(4), 1220–1229.

Marcos, S., Sawides, L., Gambra, E., & Dorronsoro, C. (2008). Influence of adaptive-optics ocular aberration correction on visual acuity at different luminances and contrast polarities. *Journal of Vision, 8*(13), 1–12.

Martin, J. A., & Roorda, A. (2005). Direct and noninvasive assessment of parafoveal capillary leukocyte velocity. *Ophthalmology, 112*(12), 2219–2224.

Martin, J. A., & Roorda, A. (2009). Pulsatility of parafoveal capillary leukocytes. *Experimental Eye Research, 88*(3), 356–360.

Masters, B. R., & Thompson, B. J. (2001). Selected papers on optical low-coherence reflectometry and tomography. SPIE milestone series, Vol. MS 165, Bellingham, Washington.

McAllister, J. T., Dubis, A. M., Tait, D. M., Ostler, S., Rha, J., Stepien, K. E., et al. (2010). Arrested development: High-resolution imaging of foveal morphology in albinism. *Vision Research, 50*, 810–817.

Merino, D., Dainty, C., Bradu, A., & Podoleanu, A. G. (2006). Adaptive optics enhanced simultaneous en-face optical coherence tomography and scanning laser ophthalmoscopy. *Optics Express, 14*(8), 3345–3353.

Miller, D. T., Kocaoglu, O. P., Wang, Q., & Lee, S. (2011). Adaptive optics and the eye (super resolution OCT). *Eye, 25*(3), 321–330.

Miller, D. T., Qu, J., Jonnal, R. S., & Thorn, K. (2003). Coherence gating and adaptive optics in the eye. *Proceedings of SPIE, 4956*, 65–72.

Miller, D. T., & Roorda, A. (2009). Adaptive optics in retinal microscopy and vision. In M. Bass, C. Decusatis, J. M. Enoch, V. Lakshminarayanan, G. Li, C. Macdonald, V. N. Mahajan, & E. Van Stryland (Eds.), *Handbook of optics* (3rd ed.. *Vision and vision optics* (3rd ed.) (Vol. III). New York: McGraw Hill.

Miller, D., Williams, D. R., Morris, G. M., & Liang, J. (1996). Images of cone photoreceptors in the living human eye. *Vision Research, 36*, 1067–1079.

Minsky, M. (1957). US patent #3013,467, described in scanning, 10, 1988, 128–138.

Morgan, J. I. W., Dubra, A., Wolfe, R., Merigan, W. H., & Williams, D. R. (2009). In vivo autofluorescence imaging of the human and macaque retinal pigment epithelial cell mosaic. *Investigative Ophthalmology and Visual Science (50)*, 1350–1359.

Mujat, M., Ferguson, R. D., Patel, A. H., Iftimia, N., Lue, N., & Hammer, D. X. (2010). High resolution multimodal clinical ophthalmic imaging system. *Optics Express, 18*(11), 11607–11621. doi:10.1364/OE.18.011607.

Neitz, J., Carroll, J., Yamauchi, Y., Neitz, M., & Williams, D. R. (2002). Color perception is mediated by a plastic neural mechanism that remains adjustable in adults. *Neuron, 35*, 783–792.

Novotny, R., & Alvis, D. L. (1961). A method of photographing fluorescence in circulating blood in the human retina. *Circulation, 24*, 82–86.

Ogle, K. N., & Rucker, C. W. (1953). Fundus photographs in color using a high speed flash tube in the Zeiss retinal camera. *AMA Archives of Ophthalmology, 49*, 435–438.

Pacques, M., Simonuti, M., Roux, M. J., Picaud, S., Levavasseiu, E., Bellman, C., et al. (2006). High resolution fundus imaging by confocal scanning laser ophthalmoscopy in the mouse. *Vision Research, 46*, 1336–1345.

Perez, G. M., Manzanera, S., & Artal, P. (2009). Impact of scattering and spherical aberration in contrast sensitivity. *Journal of Vision, 9*(3), 1–10 (article 19).

Pircher, M., Baumann, B., Göttzinger, E., & Hitzenberger, C. K. (2006). Retinal cone mosaic imaged with transverse scanning optical coherence tomography. *Optics Letters, 31*(12), 1821–1823.

Pircher, M., Zawadzki, R. J., Evans, J. W., Werner, J. S., & Hitzenberger, C. K. (2008). Simultaneous imaging of human cone mosaic with adaptive optics enhanced scanning laser ophthalmoscopy and high-speed transversal scanning optical coherence tomography. *Optics Letters, 33*(1), 22–24.

Podoleanu, A. G. (2005). Optical coherence tomography. *British Journal of Radiology, 78*(935), 976–988 (review).

Podoleanu, A. G., & Rosen, R. B. (2008). Combinations of techniques in imaging the retina with high resolution. *Progress in Retinal and Eye Research, 27*(4), 464–499 (review).

Porter, J., Queener, H., Lin, J., Thorn, K., & Awwal, A. (2006). *Adaptive optics for vision science*. Hoboken, New Jersey: John Wiley & Sons, Inc.

Putnam, N. M., Hofer, H. J., Doble, N., Chen, L., Carroll, J., & Williams, D. R. (2005). The locus of fixation and the foveal cone mosaic. *Journal of Vision, 5*(7), 632–639.

Raghunandan, A., Frasier, J., Poonja, S., Roorda, A., & Stevenson, S. B. (2008). Psychophysical measurements of referenced and unreferenced motion processing using high-resolution retinal imaging. *Journal of Vision, 8*(14), 1–11 (article 14).

Rocha, K. M., Vabre, L., Chateau, N., & Krueger, R. R. (2010). Enhanced visual acuity and image perception following correction of highly aberrated eyes using an adaptive optics visual simulator. *Journal of Refractive Surgery, 26*(1), 52–56.

Rocha, K. M., Vabre, L., Harms, F., Chateau, N., & Krueger, R. R. (2007). Effects of Zernike wavefront aberrations on visual acuity measured using electromagnetic adaptive optics technology. *Journal of Refractive Surgery, 23*(9), 953–959.

Rouger, H., Benard, Y., & Legras, R. (2009). Effect of monochromatic induced aberrations on visual performance measured by adaptive optics technology. *Journal of Refractive Surgery, 11*, 1–10.

Roorda, A. (2010). Applications of adaptive optics scanning laser ophthalmoscopy. *Optometry and Visual Science, 87*(4), 260–268 (review).

Roorda, A., Metha, A., Lennie, P., & Williams, D. R. (2001). Packing arrangement of the three cone classes in the primate retina. *Vision Research, 41*(12), 1291–1306.

Roorda, A., Romero-Borja, F., Donnelly, I. W., Queener, H., Hebert, T., & Campbell, M. (2002). Adaptive optics scanning laser ophthalmoscopy. *Optics Express, 10*(9), 405–412.

Roorda, A., & Williams, D. R. (1999). The arrangement of the three cone classes in the living human eye. *Nature, 397*(6719), 520–522.

Roorda, A., Zhang, Y., & Duncan, J. L. (2007). High-resolution in vivo imaging of the RPE mosaic in eyes with retinal disease. *Investigative Ophthalmology and Visual Science, 48*(5), 2297–2303.

Rossi, E. A., Chung, M., Dubra, A., Hunter, J. J., Merigan, W. H., & Williams, D. R. (2011). Imaging retinal mosaics in the living eye. *Eye*, 1–8.

Rossi, E. A., & Roorda, A. (2010). Is visual resolution after adaptive optics correction susceptible to perceptual learning? *Journal of Vision, 10*(12), 11.

Rossi, E. A., Weiser, P., Tarrant, J., & Roorda, A. (2007). Visual performance in emmetropia and low myopia after correction of high-order aberrations. *Journal of Vision, 7*(8), 14.

Sabesan, R., & Yoon, G. (2010). Neural compensation for long-term asymmetric optical blur to improve visual performance in keratoconic eyes. *Investigative Ophthalmology and Visual Science, 51*(7), 3835–3839.

Sawides, L., Gambra, E., Pascual, D., Dorronsoro, C., & Marcos, S. (2010). Visual performance with real-life tasks under adaptive-optics ocular aberration correction. *Journal of Vision, 10*(5), 19. doi:10.1167/10.5.19.

Schuman, J. S., Puliafito, C. A., & Fujimoto, J. G. (2004). *Optical coherence tomography of ocular diseases* (2nd ed.). Thorofare, NJ: Slack Inc (spelled "Schulman" in your doc).

Seeliger, M. W., Beck, S. C., Pereyra-Munoz, N., Dangel, S., Tsai, J. Y., Luhmann, U. F., et al. (2005). In vivo confocal imaging of the retina in animal models using scanning laser ophthalmoscopy. *Vision Research, 45*, 3512–3519.

Shroff, S., Fienup, J. R., & Williams, D. R. (2009). Phase-shift estimation in sinusoidally illuminated images for lateral superresolution. *Journal of the Optical Society of America A – Optics Image Science and Vision, 26*(2), 413–424.

Shroff, S., Fienup, J. R., & Williams, D. R. (2010). Lateral superresolution using a posteriori phase shift estimation for a moving object – Experimental results. *Journal of the Optical Society of America A – Optics Image Science and Vision, 27*(8), 1770–1782.

Sincich, L. C., Zhang, Y., Tiruveedhula, P., Horton, J. C., & Roorda, A. (2009). Resolving single cone inputs to visual receptive fields. *Nature Neuroscience, 12*(8), 967–969.

Smirnov, M. S. (1961). Measurement of the wave aberration of the human eye. *Biophysics, 6*, 687–703.

Stevenson, S. B., & Roorda, A. (2005). Correcting for miniature eye movements in high resolution scanning laser ophthalmoscopy. In F. Manns, P. Soderberg, & A. Ho (Eds.). *Ophthalmic technologies* (Vol. XI, pp. 45–151). Bellingham, WA: SPIE.

Talcott, K. E., Ratnam, K., Sundquist, S. M., Lucero, A. S., Lujan, B. J., Tao, W., et al. (2011). Longitudinal study of cone photoreceptors during retinal degeneration and in response to ciliary neurotrophic factor treatment. *Investigative Ophthalmology and Visual Science, 52*(5), 2219–2226.

Talcott, K. E., Sundquist, S., Solovyev, A., Lujan, B. J., Tao, W., Roorda, A., et al. (2010). High-resolution in-vivo imaging of cone photoreceptors in eyes treated with sustained-release ciliary neurotrophic factor in patients with retinitis pigmentosa. *Investigative Ophthalmology and Visual Science*, 51 (E-abstract 1385).

Tam, J., Martin, J. A., & Roorda, A. (2010). Noninvasive visualization and analysis of parafoveal capillaries in humans. *Investigative Ophthalmology and Visual Science, 51*, 1691–1698.

Tam, J., Tiruveedhula, P., & Roorda, A. (2011). Characterization of single-file flow through human retinal parafoveal capillaries using an adaptive optics scanning laser ophthalmoscope. *Biomedical Optics Express, 2*(4), 781–793.

Torti, C., Povazay, B., Hofer, B., Unterhuber, A., Carroll, J., Ahnelt, P. K., et al. (2009). Adaptive optics optical coherence tomography at 120,000 depth scans/s for non-invasive cellular phenotyping of the living human retina. *Optics Express, 17*(22), 19382–19400. doi:10.1364/OE.17.019382.

Vogel, C. R., Arathorn, D. W., Roorda, A., & Parker, A. (2006). Retinal motion estimation and image dewarping in adaptive optics scanning laser ophthalmoscopy. *Optics Express, 14*, 487–497.

Vohnsen, B., Iglesias, I., & Artal, P. (2004). High-resolution imaging of the in-vivo human eye retina. *Optics Letters, 29*(9), 968–970.

von Ruckmann, A., Fitzke, F. W., & Bird, A. C. (1995). Distribution of fundus autofluorescence with a scanning laser ophthalmoscope. *British Journal of Ophthalmology, 79*, 407–412.

Wade, A. R., & Fitzke, F. W. (1998). In-vivo imaging of the human cone photoreceptor mosaicusing a confocal LSO. *Lasers and Light in Ophthalmology, 8*, 129–136.

Wagner-Schuman, M., Neitz, J., Rha, J., Williams, D. R., Neitz, M., & Carroll, J. (2010). Color-deficient cone mosaics associated with Xq28 opsin mutations: A stop codon versus gene deletions. *Vision Research, 50*(23), 2396–2402.

Walsh, G., Charman, W. N., & Howland, H. C. (1984). Objective technique for the determination of monochromatic aberrations of the human eye. *Journal of the Optical Society of America A – Optics Image Science and Vision, 1*, 987–992.

Walsh, M. K., & Quigley, H. A. (2008). In vivo time-lapse fluorescence imaging of individual retinal ganglion cells in mice. *Journal of Neuroscience Methods, 169*, 214–221.

Wang, Q., Kocaoglu, O. P., Cense, B., Bruestle, J., Jonnal, R. S., Gao, W., et al. (in press). Imaging retinal capillaries using ultrahigh-resolution optical coherence tomography and adaptive optics. *Investigative Ophthalmology and Visual Science*.

Webb, R. H., Hughes, G. W., & Delori, F. C. (1987). Confocal scanning laser ophthalmoscope. *Applied Optics, 26*(8), 1492–1499. doi:10.1364/AO.26.001492.

Webb, R. H., Hughes, G. W., & Pomerantzeff, O. (1980). Flying spot TV ophthalmoscope. *Applied Optics, 19*, 2991–2997.

Werner, J. S., Keltner, J. L., Zawadzki, R. J., & Choi, S. S. (2011). Outer retinal abnormalities associated with inner retinal pathology in nonglaucomatous and glaucomatous optic neuropathies. *Eye, 25*, 279–289.

Williams, D. R. (1985). Visibility of interference fringes near the resolution limit. *Journal of the Optical Society of America A – Optics Image Science and Vision, 2*, 1087–1093.

Williams, D. R. (1988). Topography of the foveal cone mosaic in the living human eye. *Vision Research, 28*, 433–454.

Williams, D. R., & Hofer, H. (2003). Formation and acquisition of the retinal image. In L. M. Chalupa & J. S. Werner (Eds.), *The visual neurosciences* (pp. 795–810). Cambridge, MA: MIT Press.

Williams, D. R., MacLeod, D. I. A., & Hayhoe, M. M. (1981). Punctate sensitivity of the blue sensitive mechanism. *Vision Research, 21*, 1357–1376.

Williams, D., Yoon, G. Y., Porter, J., Guirao, A., Hofer, H., & Cox, I. (2000). Visual benefit of correcting higher order aberrations of the eye. *Journal of Refractive Surgery, 16*(5), S554–S559.

Wilt, B., Burns, L., Ho, E., Ghosh, K., Mukamel, E., & Schnitzer, M. (2009). Advances in light microscopy for neuroscience. *Annual Review of Neuroscience, 32*, 435–506.

Wojtkowski, M. (2010). High-speed optical coherence tomography: Basics and applications. *Applied Optics, 49*(16), D30–D61. doi:10.1364/AO.49.000D30 (review).

Wojtkowski, M., Kowalczyk, A., Leitgeb, R., & Fercher, A. F. (2002). Full range complex spectral optical coherence tomography technique in eye imaging. *Optics Letters, 27*(16), 1415–1417.

Wojtkowski, M., Leitgeb, R., Kowalczyk, A., Bajraszewski, T., & Fercher, A. F. (2002). In vivo human retinal imaging by Fourier domain optical coherence tomography. *Journal of Biomedial Optics, 7*(3), 457–463.

Wolfing, J. I., Chung, M., Carroll, J., Roorda, A., & Williams, D. R. (2006). High-resolution retinal imaging of cone-rod dystrophy. *Ophthalmology, 113* (1019.e1).

Yang, Q., Arathorn, D. W., Tiruveedhula, P., Vogel, C. R., & Roorda, A. (2010). Design of an integrated hardware interface for AOSLO image capture and cone-targeted stimulus delivery. *Optics Express, 18*, 17841–17858.

Yin, L., & Williams, D. R. (2011). Adaptive optics. In J. C. Behearse & D. Bok (Eds.), *The retina and its disorders*. Academic Press.

Yoon, G. Y., & Williams, D. R. (2002). Visual performance after correcting the monochromatic and chromatic aberrations of the eye. *Journal of the Optical Society of America A – Optics Image Science and Vision, 19*(2), 266–275.

Yoon, M. K., Roorda, A., Zhang, Y., Nakanishi, C., Wong, L. J., Zhang, Q., et al. (2009). Adaptive optics scanning laser ophthalmoscopy images in a family with the mitochondrial DNA T8993C mutation. *Investigative Ophthalmology and Visual Science, 50*, 1838–1847.

Young, T. (1801). On the mechanism of the eye. *Philosophical Transactions of the Royal Society of London, 91*(Part I) (23–88 + plates).

Young, T. (1804). Experimental demonstration of the general law of the interference of light. *Philosophical Transactions of the Royal Society of London, 94*, 1–16.

Zawadzki, R. J., Cense, B., Zhang, Y., Choi, S. S., Miller, D. T., & Werner, J. S. (2008). Ultrahigh-resolution optical coherence tomography with monochromatic and chromatic aberration correction. *Optics Express, 16*(11), 8126–8143.

Zawadzki, R. J., Choi, S. S., Jones, S. M., Oliver, S. S., & Werner, J. S. (2007). Adaptive optics-optical coherence tomography: Optimizing visualization of microscopic retinal structures in three dimensions. *Journal of the Optical Society of America A – Optics Image Science and Vision, 24*(5), 1373–1383.

Zawadzki, R. J., Jones, S. M., Olivier, S. S., Zhao, M., Bower, B. A., Izatt, J. A., et al. (2005). Adaptive-optics optical coherence tomography for high-resolution and high-speed 3D retinal in vivo imaging. *Optics Express, 13*(21), 8532–8546.

Zhang, Y., Cense, B., Rha, J., Jonnal, R. S., Gao, W., Zawadzki, R. J., et al. (2006). High-speed volumetric imaging of cone photoreceptors with adaptive optics spectral-domain optical coherence tomography. *Optics Express, 14*(10), 4380–4394.

Zhang, Y., Rha, J., Jonnal, R. S., & Miller, D. T. (2005). AO parallel spectral domain optical coherence tomography for imaging the living retina. *Optics Express, 13*, 4792–4811.

Zhong, Z., Petrig, B. L., Qi, X., & Burns, S. A. (2008). In vivo measurement of erythrocyte velocity and retinal blood flow using adaptive optics scanning laser ophthalmoscopy. *Optics Express, 16*(17), 12746–12756.

Zhong, Z., Song, H., Chui, T. Y., Petrig, B. L., & Burns, S. A. (in press). Non-invasive measurements and analysis of blood velocity profiles in human retinal vessels. *Investigative Ophthalmology and Visual Science*.